SEVENTH FRAMEWORK PROGRAMME

THEME FP7-ICT-2009-C

Instrument	STREP
Project no.	244068
Project acronym	**CROSSTRAP**
Project title	**C**oherently-enhanced **R**aman **O**ne-beam **S**tandoff **S**pectroscopic **TR**acing of **A**irborne **P**ollutants

Deliverable D5.2

Year 2 Periodic Report

Due date of deliverable	month 24
Actual submission date	26/03/2012
Start date of project	01/02/2010
Duration of the project	36 months
Organization name of lead contractor for this deliverable	**TU WIEN**
Dissemination Level	public

CROSSTRAP
Deliverable D5.2

PROJECT PERIODIC REPORT

Grant Agreement number: 244068

Project acronym: CROSS TRAP

Project title: Coherently-enhanced Raman One-beam Standoff Spectroscopic TRacing of Airborne Pollutants

Funding Scheme: STREP

Date of latest version of Annex I against which the assessment will be made:

Periodic report: **1st** ☐ **2nd** ☑ **3rd** ☐ **4th** ☐

Period covered: **from 01.02.2011 to 31.01.2012**

Name, title and organisation of the scientific representative of the project's coordinator: Andrius Baltuska, Photonics Institute, Vienna University of Technology

Tel: +436646 0588 3876

Fax:+43 1 58801 387 99

E-mail: baltuska@tuwien.ac.at

Project website address: www.crosstrap.eu

Declaration by the scientific representative of the project coordinator

I, as scientific representative of the coordinator of this project and in line with the obligations as stated in Article II.2.3 of the Grant Agreement declare that:

- The attached periodic report represents an accurate description of the work carried out in this project for this reporting period;
- The project (tick as appropriate) [1]:

  ☐ has fully achieved its objectives and technical goals for the period;

  ☑ has achieved most of its objectives and technical goals for the period with relatively minor deviations.

  ☐ has failed to achieve critical objectives and/or is not at all on schedule.

- The public website, if applicable

  ☑ is up to date

  ☐ is not up to date

- To my best knowledge, the financial statements which are being submitted as part of this report are in line with the actual work carried out and are consistent with the report on the resources used for the project (section 3.4) and if applicable with the certificate on financial statement.
- All beneficiaries, in particular non-profit public bodies, secondary and higher education establishments, research organisations and SMEs, have declared to have verified their legal status. Any changes have been reported under section 3.2.3 (Project Management) in accordance with Article II.3.f of the Grant Agreement.

Name of scientific representative of the Coordinator: .....Andrius Baltuska.....

Date: ....28..../ ..03...../ 2012.....

For most of the projects, the signature of this declaration could be done directly via the IT reporting tool through an adapted IT mechanism.

[1] If either of these boxes below is ticked, the report should reflect these and any remedial actions taken.

3.1 Publishable summary

CROSS TRAP (Coherently-enhanced Raman One-beam Standoff Spectroscopic Racing of Airborne Pollutants) in an FP7 STREP project within the Future and Emerging Technologies Open Scheme. The project is coordinated by Prof. Andrius Baltuska, Photonics Institute, Vienna University of Technology (TU WIEN), Austria (email baltuska@tuwien.ac.at) and includes the following contractors:

• Politecnico di Milano	POLIMI,	Italy
• Menlo Systems GmbH	MSG,	Germany
• Covesion Ltd.	CL,	UK
• Light Conversion, Ltd	LC,	Lithuania
• Ruprecht-Karls Univ. Heidelberg	UHEI,	Germany
• Internation Laser Center of Moscow State Univ.	ILC MSU,	Russia
• Bilkent Univ.	BILKENT	Turkey

The project website is www.crosstrap.eu.

Project CROSS TRAP tackles the ICT objective of photonic components and subsystems for sensing for environment, well-being safety and security. The project aims at developing a versatile method and apparatus for standoff chemical identification of trace amounts of airborne pollutants, such as biochemicals, bacterial threats and explosive materials that can be fingerprinted using their characteristic vibrational Raman spectral signatures. The core idea of the proposal is to enable a free-space scheme for coherent stimulated Raman scattering (SRS) in the direction almost exactly reversed with respect to an outgoing laser excitation, so that the probe beam can be arbitrarily pointed in any unobstructed direction and an enhanced backward propagating signal detected at the laser source using a LIDAR-type apparatus.

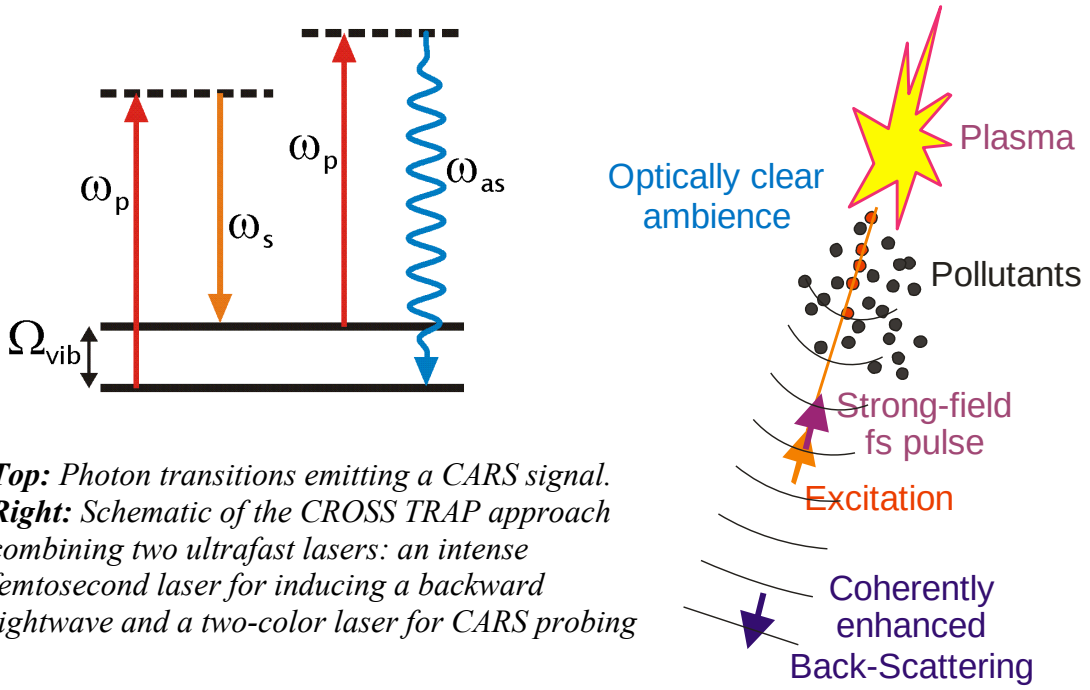

Top: *Photon transitions emitting a CARS signal.*
Right: *Schematic of the CROSS TRAP approach combining two ultrafast lasers: an intense femtosecond laser for inducing a backward lightwave and a two-color laser for CARS probing*

The radical advantage, as compared to incoherent light probing techniques, lies in coherent enhancement, which implies that light fields are phase-matched, i.e. added in phase, so that the signal propagation is confined to very narrow solid angle and the signal magnitude scales quadratically with interaction length and the concentration of the resonantly vibrationally excited

molecules. In order to enable the generation of backward SRS signal, a backward propagating laser field must be supplied in the form of a reflected/re-scattered fraction of the incident beam or as a beam generated through lasing in air.

The grand technological and scientific challenge in CROSS TRAP is to realize a free-space SRS relying on the air itself as a medium emitting a back-propagating beam that facilitated phase-matching. The emission of the laser-like backward beam is a product of a reversible interaction of gas with a strong field of an ultrashort intense laser pulse that leaves in its wake a string of ionized gas (plasma) called a light filament.

In the context of CROSS TRAP, such an artificially enhanced and remotely controlled backward emitting process serves as an enabling mechanism for moving away from an incoherent wide-angle signal harvesting in a LIDAR-type probing technique toward a coherent, and thereby stronger and less-divergent, beam detection. In a broader sense, far beyond the scope of CROSS TRAP, an ability to induce and control light reflection from an isotropic pure transparent gas would undoubtedly trigger the development of new free-space techniques in the areas of remote sensing, ranging, target illumination, chemical marking and, not unlikely, for eavesdropping on free space optical communications.

The objectives of this project are:

-demonstration of a controlled atmospheric "back-emitter" by creating and optimizing plasma filaments in air;

-development of a synchronized SRS detection and identification scheme employing a back-propagating beam geometry facilitated by the filament;

-development of a fully functioning prototype for a stand-off distance of hundreds of meters based on a dual laser chain (a femtosecond high-energy mid-IR for filament generation and a 0.5-GHz burst mode rate laser for SRS probing);

-feasibility demonstration of a scheme for filament excitation with a laser operating at an eye-safe infrared wavelength.

During the second year of the project, the synergetic effort of the CROSS TRAP Consortium resulted in the following main achievements:

- **Realization of backward emission in the shape of free-space lasing of Nitrogen gas in a single femtosecond filament using intense near-IR and mid-IR pump laser pulses** (***Project Milestone 3***, leading partner TU Wien in cooperation with ILCMSU). We have achieved remarkably efficient backward lasing from a mixture of nitrogen and argon which results in the generation of ~3-μJ UV pulses at the transitions of the molecular Nitrogen laser at 337 nm and 357 nm. Subsequently, by adopting a novel mid-IR intense femtosecond pulse source, we were able to eliminate argon as a mediator in the inversion creation scheme. As a result, we were able to generate sub-μJ UV pulses from nitrogen and observe both molecular N_2 emission and molecular ion, N_2^+, emission at their respective wavelengths.

- **Confirmation of the possibility to obtain backscattering from multiple filaments**, which dramatically broadens the range of opportunities for the envisaged technique, because it makes it possible to overcome the inherent limitation of a single filament caused by the phenomenon of intensity clamping (***Project Milestone 4***, leading partner TU Wien in cooperation with UHEI). We have shown that by using phase shaped near-IR pulses it is possible to have a dramatic enhancement of the lasing and amplification properties in the regime of multiple filaments thus bypassing the pulse energy limitation set by a single filament condition.

• **Development of an efficient scheme for non-resonant background suppression in coherent Raman scattering spectroscopies** (***Project Milestone 5***, leading partner UHEI, in cooperation with POLIMI**).** Here, we introduce new setups for multiplex coherent Raman Scattering, developed by the project partners, which are both studying new ways to obtain background suppression. One is using the concept of single-beam CARS with pulse shaping which allows the extraction of the pure linear Raman spectra without any theoretical treatment. The second setup introduces a new modality of coherent Raman scattering, which we call Balanced Detection Raman Induced Kerr Effect (BD-RIKE), that combines the advantages of CARS (absence of linear background) with those of SRS (suppression of the non-resonant response, linear scaling with concentration).

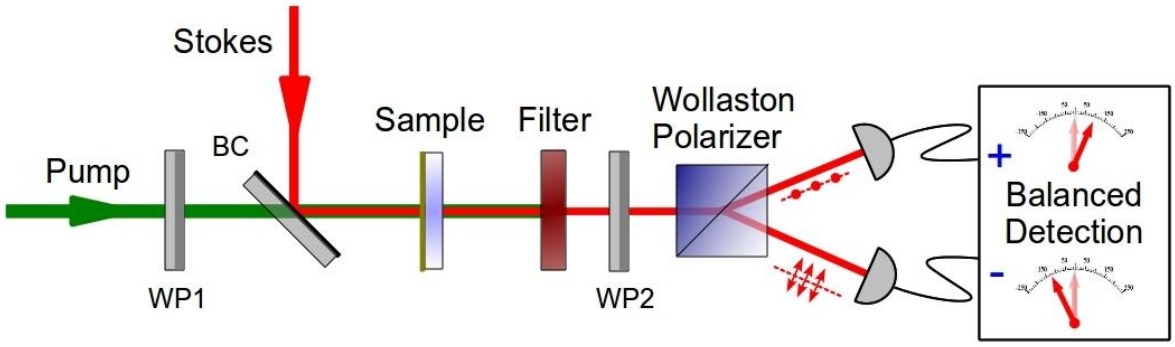

Conceptual scheme for a BD-RIKE experiment. WPs: waveplates.

• **Development of a burst mode fiber amplifier for target interrogation in the backward probing geometry (*Project Milestone 7*,** leading partner Bilkent, in cooperation with MSG**).** The necessity of implementing a burst-mode laser with closely spaced micropulses within each burst is dictated by the backward propagating beam geometry of the envisaged CROSS TRAP apparatus in which the interrogating pulse runs through the seed pulse from the filament emission and therefore only samples a very short distance in space corresponding to a half of the pulse width. To increase the probing depth, a train of pulses has to be shot at the incoming seed pulse from the filament emission. A corresponding micro-Joule level laser system was developed on the basis of a 0.5-GHz seeder designed by Menlo and a fiber burst amplifier developed in Bilkent.

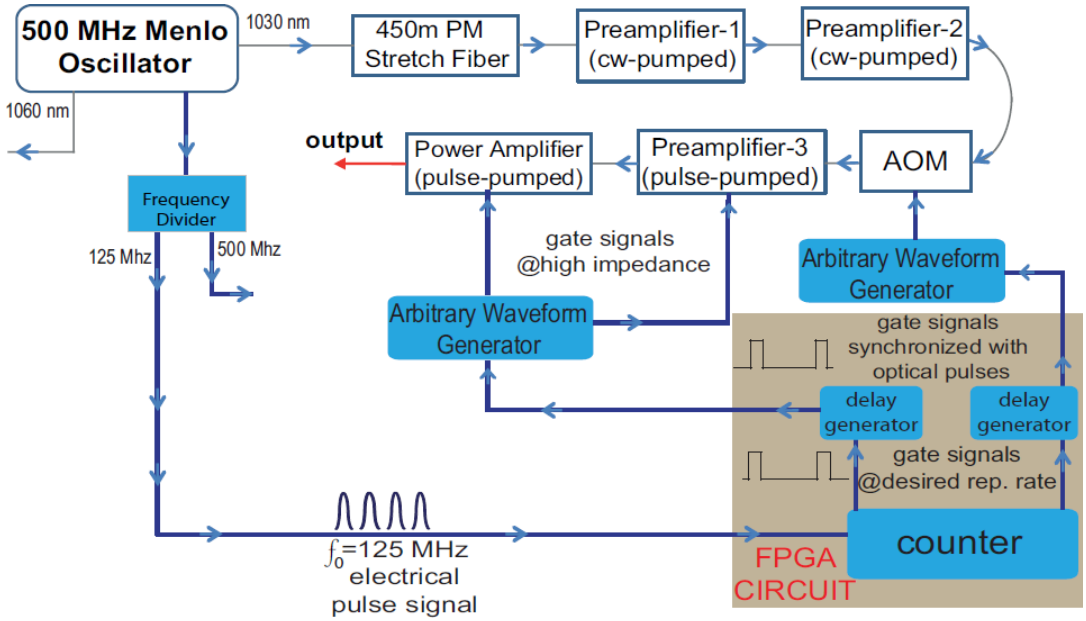

Functional diagram of the BILKENT amplifier system with the 500 MHz Menlo (MSG) oscillator as the seed source.

The consortium has deviated from its original plan to employ a 100-mJ 1-kHz repetition rate Yb amplifier both as a source of intense pulses for filamentation in air and a pump source for an eye-safe parametric amplifier. Pump-wavelength-dependent studies of the free-space backward-emitting nitrogen laser have revealed very significant advantages of employing mid-IR pump pulses rather than the 1-μm pulses that seemed to be the only technically viable option at the outset of the project. As a result, the consortium has suspended the execution of **Project Milestone 6**, the development of a 1-kHz 100-mJ Yb laser and channeled its efforts into boosting the energy of a mid-IR femtosecond OPA operating at the wavelength of 4 μm. This mid-IR system is currently the only known source capable of forming mid-IR filaments in gas. However, the pulse energy, which was increased in the second year of the project to 12 mJ is still insufficient to obtain filamentation at atmospheric pressure because the available peak power of ~130 GW is still approximately a factor of 2 below the expected critical power of self focusing at 1 bar. The ability to realize full-fledged filamentation and backward lasing in air is expected to be achieved in the third year of the project after upgrading the picoseconds pump laser energy from 300 mJ to 1 J. In light of these developments, **Project Milestone 6** has become irrelevant to the success of the project.

The results of CROSS TRAP are going to be exploited by the SMEs involved in the Consortium. The developments of two unique femtosecond laser systems will allow MSG and LC, who specialize in fiber and solid-state amplifier and parametric amplifier technology, respectively, to upgrade the performance of their commercially offered laser systems and potentially launch new laser products. CL, who specialize in frequency conversion using periodically poled crystals, have developed new crystal types for this project which can also be commercialized as standalone or products or parts of integrated frequency conversion systems.

3.2 Core of the report for the period: Project objectives, work progress and achievements, project management

3.2.1 Project objectives for the period

The overall objective of the project is to develop a method and apparatus for standoff CRS in air or gas. Several variants of stimulated Raman scattering techniques are under investigation. CARS was indicated as a method of choice in the DoW. The main challenge with this technique in the backward beam geometry is the inherent absence of collinear phase-matching for a non-degenerate case. While the search for possible phase matching solutions for backward CARS phase matching continues on the theory level (cf. Appendix in D2.2), the consortium in the second year has also performed investigation of other suitable coherent Raman implementations, such as a two-pulse (anti-)collinear pump-probe leading to the appearance of stimulated Raman gain (SRG) and loss (SRL) signals. The main prerequisite for enabling free-space backscattering in the gas phase in the absence of a scattering or reflecting medium or object is a light pulse generated as a result of interaction of a pump laser pulse with air. Since the start of the project, the consortium is exploring one type of backward emission via lasing of an inverted transition in the plasma channel formed by femtosecond filamentation of an intense near-IR and, added in the second year, mid-IR laser pulse.

Line 1: **Engineering of enhanced atmospheric backscattering (WP1),**

Line 2: **Characterization, integration, and optimization of backward-enhanced coherent Raman scattering LIDAR (WP2),**

Line 3: **Development of laser and pulse delivery systems (WP3 and WP4).**

The objective of WP1 is the development of an atmospheric backscatterer stimulated via nonlinear optical interaction with an intense femtosecond driver pulse. The following research tasks are planned for the reporting period (T0 — T0+12):

T1.3 Multifilament regime (TU WIEN, months 12-36)

T1.4 Multipulse filamentation control (TU WIEN, months 12-36)

The results of this work are summarized in the submitted deliverable **D1.2** (**Report on Laboratory-scale backscattering**. (Responsible partner TU WIEN, month 24)).

The objective of WP2 is the implementation of CARS detection. Three tasks were pursued during the reporting period:

T2.2 Modelling of CARS response (ILC MSU, UHEI, months 1-18). The objective is to develop a numerical code for simulating the CARS process, excited by narrowband picosecond pump and tunable Stokes pulses, in a variety of gaseous mixtures.

T2.3 Forward detected CARS with gaseous samples (UHEI, POLIMI, months 1-18).

The objective of this task is to test tunable narrowband picosecond pulses generated by the spectral compression method developed in WP4, in T4.4-T4.6, to drive forward CARS at short distances.

T2.4 CARS signal enhancement and non-resonant background suppression (UHEI, POLIMI, months 19-36).

T2.5 Backward detected CARS using hard surface reflection. (UHEI, POLIMI, Months 12-36).

T2.6 Standoff CARS using filament enhanced backscattering. (TU WIEN, POLIMI, UHEI, Months 19-36)

The execution of T2.5 and T2.6 was effectively merged with the following modifications to the original plan: 1) the three-pulse CARS approach, for which we cannot provide a viable solution for the phase-matching problem, was replaced by a two-pulse SRG/SRL pump-probe. 2) The use of filament backscattering will commence in Year 3. In the second year, we mimicked the emission of the nitrogen 337-nm UV laser by picosecond and nanosecond pulses from frequency-tripled Nd:YAG and Yb:KGW lasers (354.7 and 343 nm).

The core findings of the tasks performed in WP2 are summarized in the submitted deliverable **D2.2** (**Report on Background Scattering Suppression in CRS** (Responsible partner UHEI, month 24)).

The objective of WP3 is the developments of a femtosecond pump laser for filamentation. The generated filament should be optimized for free-space nitrogen emission. In light with the findings in WP1 (optimum parameters for free-space lasing) and reviewers' recommendations after the 1st year review meeting (criticism of the high-repetition rate but low pulse energy approach), the Consortium has abandoned the plan for a 100-mJ 1-kHz Yb laser in favour of a mid-IR OPA that, as a result of wavelength-dependent ponderomotive energy scaling, is capable to produce high-kinetic-energy plasma electrons (~48 eV for λ=4 μm as opposed to ~2 eV fro λ=0.8 μm).

The development of the pump source for filamentation is summarized in the submitted deliverable **D3.2** (**Driver laser for initiation of remote lasing** (Responsible partner TU Wien, month 24)).

The objective of WP4, the second WP related to laser development, is to come up with a high-repetition-rate laser system for CARS detection.

Two tasks were pursued in WP4 during the reporting period:

T4.3 High power amplification of fs pulses (MSG, BILKENT 7-36)

T4.4 Generation of tunable picosecond pulses by spectral compression (POLIMI, CL, months 1-12).

The findings of T4.3 are summarized in the submitted deliverable D4.2 (**Report on the high performance fiber laser source with novel pulse burst characteristics** (Responsible partner BILKENT, month 24).

The reason to continue T4.4 beyond its originally scheduled termination date is the potential problem with the wavelength of the free space laser. The fact that the eventual free-space backward lasing wavelength will be one of the N_2 emission UV lines (337 nm being the most prominent line) was not known at the outset of the project. Although the method of spectral compression proposed by POLIMI works very well in periodically poled crystals in the visible, its UV application is expected to be challenging due to photorefractive damage of PPLN crystals produced by CL. In addition to the bulk crystal spectral compression scenario described in D2.2, Light Conversion pursued a more elaborate approach to spectral compression based on sum-frequency generation of pulses with inverted chirps. An update on this activity is added in this periodic report.

3.2.2 Work progress and achievements during the period

Here we provide a concise overview of the progress of the work in line with the structure of Annex I to the Grant Agreement (Description of Work).

Progress in WP1 ("NLO Mirror")

Here we mentioned several key findings presented in Deliverable D1.2.

High-energy filament-excited backward N_2 laser in the Bennett scheme. The results of the free-space lasing characterization under a 4μm filament excitation are summarized in Fig. 1. Below the lasing threshold, a well-known UV fluorescence spectrum of N_2 was observed from the gas cell (Fig. 1a). At the input mid-IR pulse energy of 7 mJ, backward UV nitrogen lasing from the gas cell was observed at the nitrogen pressure above 0.3 bar and the argon pressure above 3 bar. Stimulated emission from nitrogen in the forward direction in this set of experimental measurements was not studied.

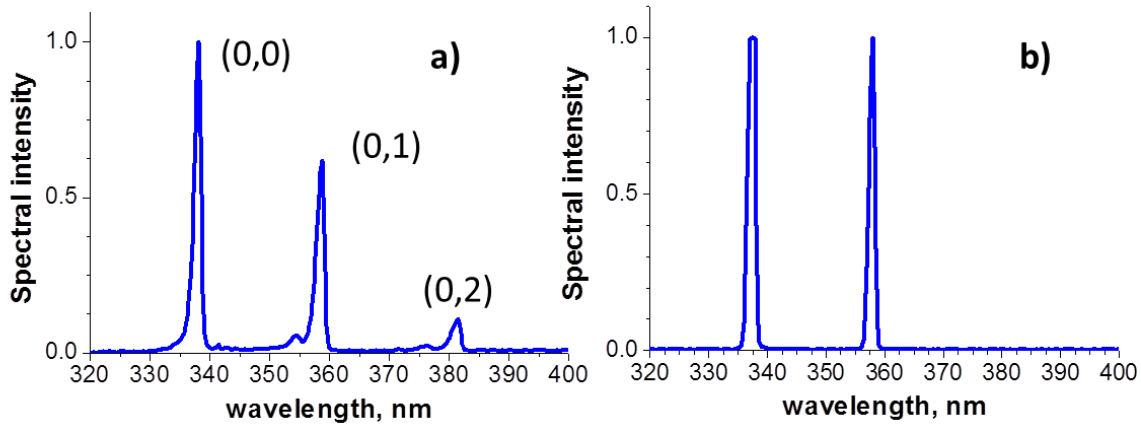

Fig. 1. Spectra of (a) fluorescence from 1 bar of pure nitrogen and (b) lasing from the 1 bar of N_2 and 5 bars of Ar mixture. Vibrational levels for C-B electronic transition are assigned.

Lasing was achieved simultaneously for two lines at 337 nm and 357 nm, belonging to the second-positive-band of N_2. These lines correspond, respectively, to the transitions from the lowest vibrational level of the upper $C^3\Pi_u$ state to the lowest and first excited vibrational levels of the $B^3\Pi_g$ electronic state (Fig.1b). At a fixed nitrogen pressure, the lasing efficiency increases with the increase of argon pressure and saturates at around 6 bar. At a fixed argon pressure, first the lasing efficiency increases with the increase of nitrogen pressure and then drops after passing a broad maximum at around 1.7 bar. For the optimal mixture (1 bar of N_2 and 5 bar of Ar), the measured sum energy at 337 and 357 nm lines reached up to 3.5 μJ, corresponding to a 0.5% energy conversion efficiency from the mid-infrared laser pulse to UV radiation. For comparison, in a discharge-pumped laser, typically less than 0.1% of the electric energy in the discharge is converted into the laser emission.

The temporal profiles of the N_2 laser pulses at 337 and 357 nm are presented in Fig.2a alongside the response function of the fast photodiode used in the measurement. Interference filters with peak transmission at 340 and 360 nm and FWHM of 10 nm were used to acquire individual temporal profiles at the two emission lines. As evidenced by Fig.24a, lasing at 337 nm develops about a nanosecond earlier than at

357 nm and is emitted as a shorter sub-ns pulse, whereas the duration of 357 nm pulse is about 2 ns FWHM. The measured spatial beam profile is shown in Fig.2b and roughly has a super-Gaussian shape. Low beam divergence of about 1.6 mrad was retrieved by measuring the beam profile as a function of the distance from the gas cell. Insertion of a 2mm- thick CaF_2 parallel plate in the beam results in appearance of clearly seen interference fringes (insert on Fig.2b) proving a high temporal coherency of the generated UV emission.

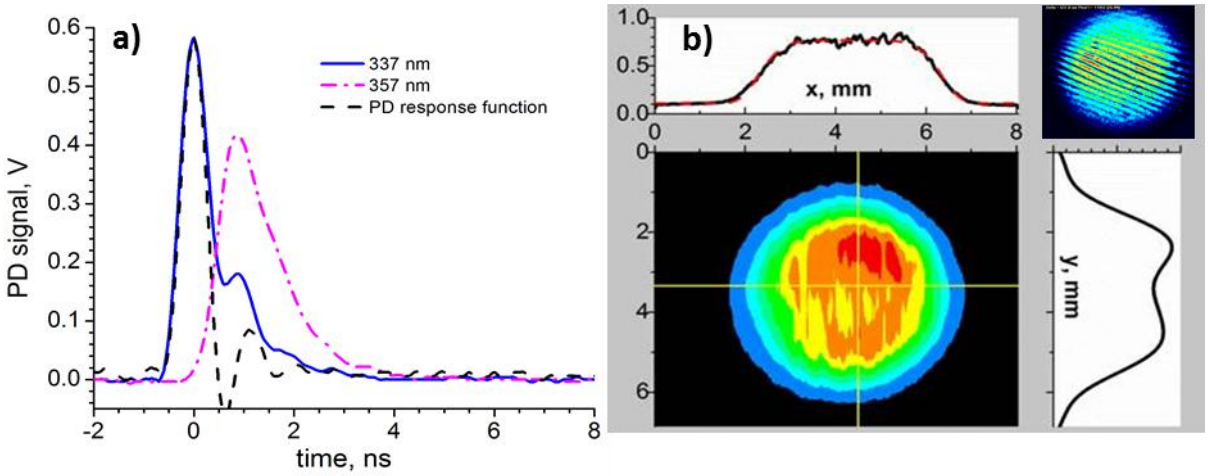

Fig. 2 (a) Temporal profiles of the 337-nm (blue solid curve) and 357-nm (magenta dash-dotted curve) laser pulses from the nitrogen–argon mixture. The dashed black line shows the photodiode response. (b) The UV-lasing beam profile. The red dotted line shows a 6^{th}-power super-Gaussian fit. Insert in b) is a CCD image of interference in the beam from a 2mm-thick CaF_2 parallel plate.

Lasing in pure N_2. Our experiments in the nitrogen-argon gas mixture have demonstrated that a mid-infrared femtosecond laser filament can induce backward-directed lasing of molecular nitrogen via a resonant excitation transfer mechanism. We have shown that a filament-assisted nitrogen laser can be at least as efficient as its conventional discharge-pumped counterpart. Also, Mid-IR ultrashort laser pulses have been shown to radically enhance filamentation-assisted lasing of N_2 relative to ultrashort pulses in the near-IR. However, the major step towards realization of UV lasing in nitrogen under atmospheric conditions would be a proof of a possibility to realize electron-impact mechanism of population inversion in nitrogen under conditions of mid-IR filament.

The scheme of the experimental setup is presented in Fig.3. The 80-fs, 8-mJ pulses at a 20-Hz repetition rate at the wavelength of 3.9 μm where focused in the gas cell filled by pure nitrogen under various pressures. Before filling nitrogen, the cell was pumped out down to $5 \cdot 10^{-2}$ mbar. We used different focusing lenses with focal lengths in the range of 20 cm – 100 cm, observing transition from short laser sparks in the gas for the case of sharp focusing (f<50 cm) to the filament formation for loose focusing. Although the laser system provides femtosecond pulses with the peak power on the level of 100 GW, it is still not high enough to overcome self-focusing threshold (our estimation of critical power at 4 μm wavelength is about twice higher). Therefore, we inevitably forced to use high gas pressures in the cell to achieve filamentation. The lifetime of the upper excited lasing state in nitrogen is about 1-2 ns for 1 bar of partial pressure and scales inversely proportional to the pressure. Thus, the gain for forward-propagating lasing in nitrogen under high

pressure conditions becomes substantially higher than for the backward direction, as it is known well in the discharge-pumped nitrogen lasers. That is why we concentrated our efforts on lasing detection in the forward direction. A several mm block of fused silica was used to absorb 4 μm laser radiation after the cell. Then, a set of interference filters was used to block harmonics of the fundamental wavelength and spectral continuum generated in the gas. A fast photodiode, a spectrometer and a CCD camera were used, respectively, for the temporal, spectral and spatial characterization of nitrogen lasing.

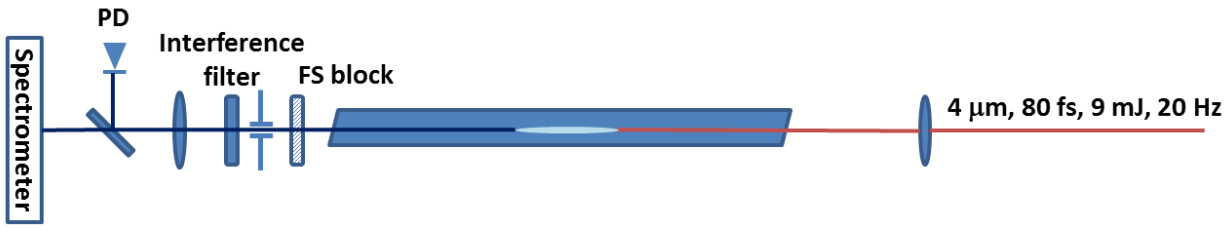

Fig. 3 *Experimental setup for forward lasing measurements from a mid-IR filament in pure nitrogen.*

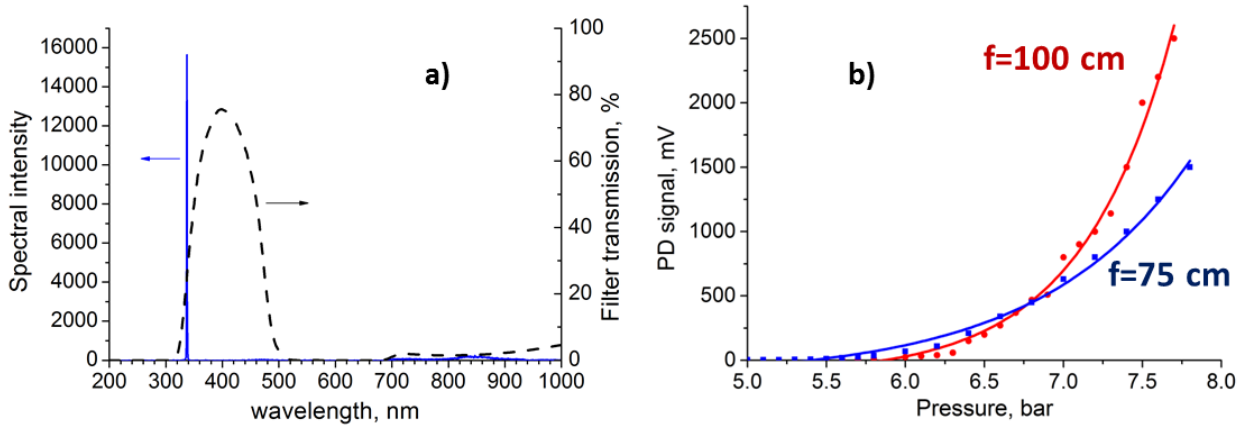

Fig. 4 *a) Spectrum of UV lasing from 6.7 bars of pure nitrogen (blue line) and spectral transmission of the interference filter (dotted line); b) pressure dependence of lasing intensity for f=100 cm focusing lens (red dots) and for f=75 cm focusing lens (blue dots). Solid lines are exponential fits.*

Using an f=100 cm lens to create a filament, laser generation in nitrogen at 337 nm wavelength was achieved for the gas pressures starting from 6 bars. The spectrum of the generated UV emission is presented in Fig. 4a. The pressure dependence of the lasing, presented in Fig. 4b, has been measured with a fast photodiode. At high pressures, necessary to achieve filamentation and lasing in our experiments, generated UV pulses have duration on the order of several hundreds of picoseconds which is beyond the temporal resolution of the photodiode. That is why the complete temporal characterization of the UV emission was not possible. The dependence of the UV yield on the gas pressure *p* can be very well fitted by the exponential law $\propto exp\left(\alpha\sqrt{p}\right)$, as it is shown in Fig. 4. This can be explained by the following arguments. The lifetime of the upper lasing has reciprocal dependence on the gas pressure and, hence, the stimulated emission crossection σ in the gain expression $g = \sigma N l$. However, the collisional probability and, therefore, the population

inversion density grow proportionally to the pressure. As a result, pressure dependence of these two products cancels each other in the gain expression. In the same time, the filament length and correspondingly the amplification length are increasing proportionally to $\sqrt{p}$, resulting in roughly the same overall law of the gain dependence on the gas pressure.

The spatial structure of the generated UV light is presented in Fig. 5. The beam divergence of about 5.6 mrad was retrieved by measuring the beam profile as a function of the distance from the gas cell in the case when the filament was formed by the f=100 cm focusing lens. Measurements with different focusing lenses have shown that the beam spatial structure depends on the focusing conditions. For loose focusing the beam always has demonstrated a donut-like structure. For relatively sharp focusing, the beam had a bell-shape structure close to the Gaussian profile. One of possible explanations for this focusing conditions dependence might be the beam refraction on plasma undergoing hydrodynamic expansion. To prove this, we plan to extend our zero-dimensional plasma kinetics model to a two-dimensional cylindrically symmetric model which will include transversal dynamics and longitudinal distribution of the plasma.

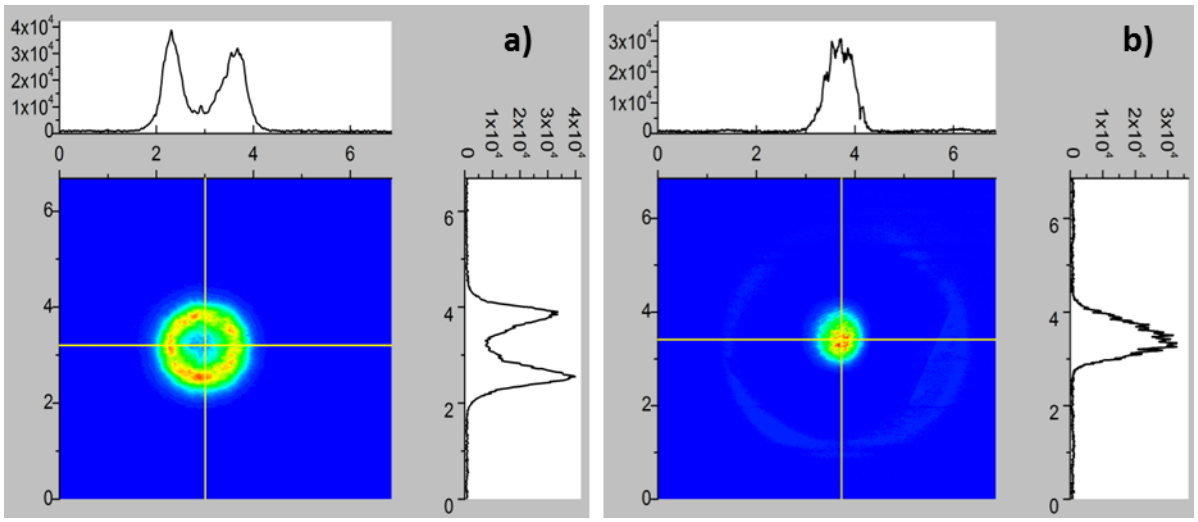

Fig. 5 *Spatial structure of the 337 nm generated beam from a mid-IR filament in 6.7 bars of pure nitrogen for a) f=100 cm focusing lens and b) for f=50 cm focusing lens.*

To measure the efficiency of the lasing, we used a UV photodiode calibrated with a home-made OPA picosecond laser system providing several micro-joules energy at 337 nm wavelength. Including the correction for the interference filter transmission, we determined that about 60 nJ of energy is emitted in the 337 nm generated beam under 7 bars of nitrogen pressure.

Multipulse, multifilamentation enhancement. As it was pointed out before, realization of electron collision pumping mechanism in nitrogen under conditions of near-IR filament is a very challenging task and intrinsically requires control over parameters of the filament plasma. Methods of an adaptive control, used before in the filamentation physics for controlling parameters of the generated spectral continuum, might be used as a powerful tool for this purpose. We performed set

of experiments applying for the first time, to the best of our knowledge, adaptive control over the efficiency of UV fluorescence from nitrogen in a near-IR femtosecond filament using a spatial light-modulator (SLM).

Experiments were performed with a home-made 0.5-kHz repetition rateYb:CaF_2 laser, providing 220 fs, 7 mJ, 1.03 μm pulses. The pulse shaper, based on SLM embedded in a 4*f* optical setup with cylindrical mirrors (Fig.6), was installed after the stretcher, before the regenerative amplifier. The shaped laser pulses were focused with an *f*=1m focusing lens into a 1.5-m-long gas cell with transparent sidewalls and Brewster input and output windows made of CaF_2. After a pumpdown to $5 \cdot 10^{-2}$ mbar, the cell was filled up with nitrogen under various pressures.

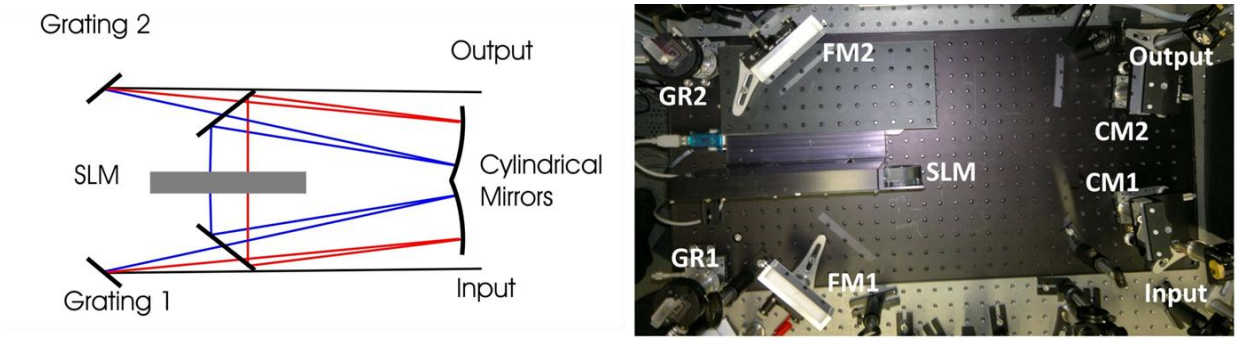

Fig. 6 *SLM optical layout (left) and photo (right).*

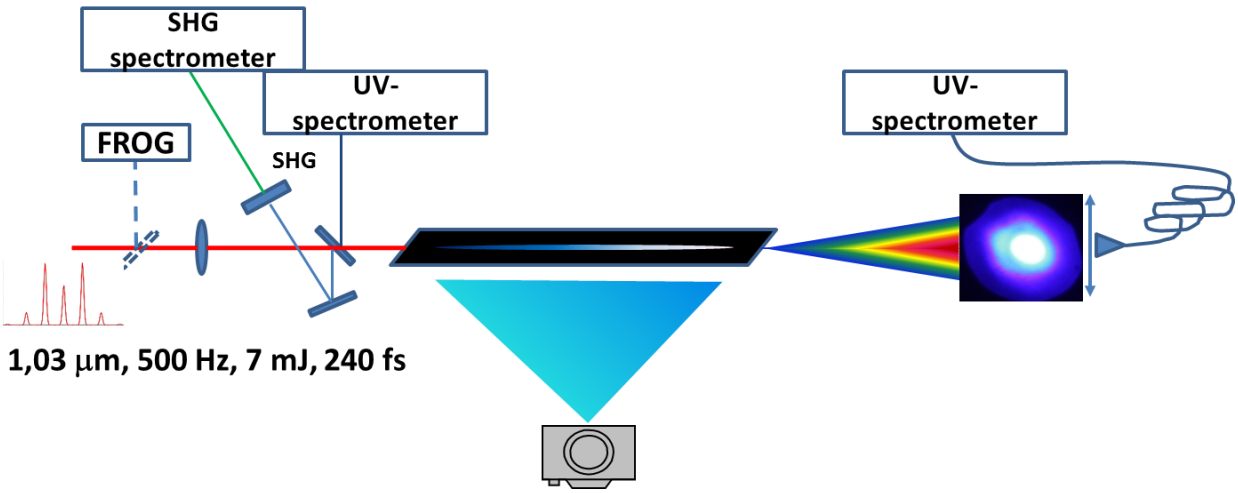

Fig. 7 *Experimental setup for adaptive control over fluorescence in the near-IR filament*

The detection of the weak UV fluorescence from nitrogen requires collection of the fluorescence emission by focusing optics and relatively long acquisition times. This was possible only in backward direction as the strong background of white-light continuum, generated inside the filament, obscures forward detection of the fluorescence. To detect fluorescence in the backward direction, the laser beam was focused into the cell through a 2mm thick, 45° dichroic mirror with a ~90% transmission efficiency for 1.03 μm radiation and a >95% reflection efficiency in the range of 335 nm-500 nm. The fluorescence signal, reflected off the dichroic mirror, was focused on the entrance slit of the UV spectrometer with a highly efficient CCD camera as a detector.

For the detection of the emission in the forward direction, the central high-intensity filament part of the beam was blocked off and the annular transmitted beam was scanned by moving the entrance slit of an HR-4000 Ocean Optics spectrometer attached to an XY positioning stage. The input pulse sequence created by the SLM was characterized by SHG-FROG in front of the focusing lens. Also, as a reference signal to control the pulse sequence generated by the SLM, a small portion of the input energy reflected by the dichroic mirror was used for the SHG in the 100 μm-thick BBO crystal and the SHG-signal was detected by the second spectrometer in-line with the fluorescence spectrum. Additionally to the spectral measurements, we used a digital photo-camera for the side-view visualization of the filament. The details of the experimental setup are presented in Fig. 7.

To control fluorescence emission from nitrogen, we applied a sinusoidal mask $\varphi(\omega) = \mathrm{asin}\,(\omega\tau + c)$ to the spectral phase of the compressed laser pulse, where a determines the relative amplitudes and the number of pulse replicas (Fig. 8) and τ the temporal delay between them [Zeidler01]. The idea behind the use of such a pulse train is that relatively weak pre-pulses in the train can effectively align molecular nitrogen at pulse separations corresponding to fractional revivals of the rotational wavepacket.

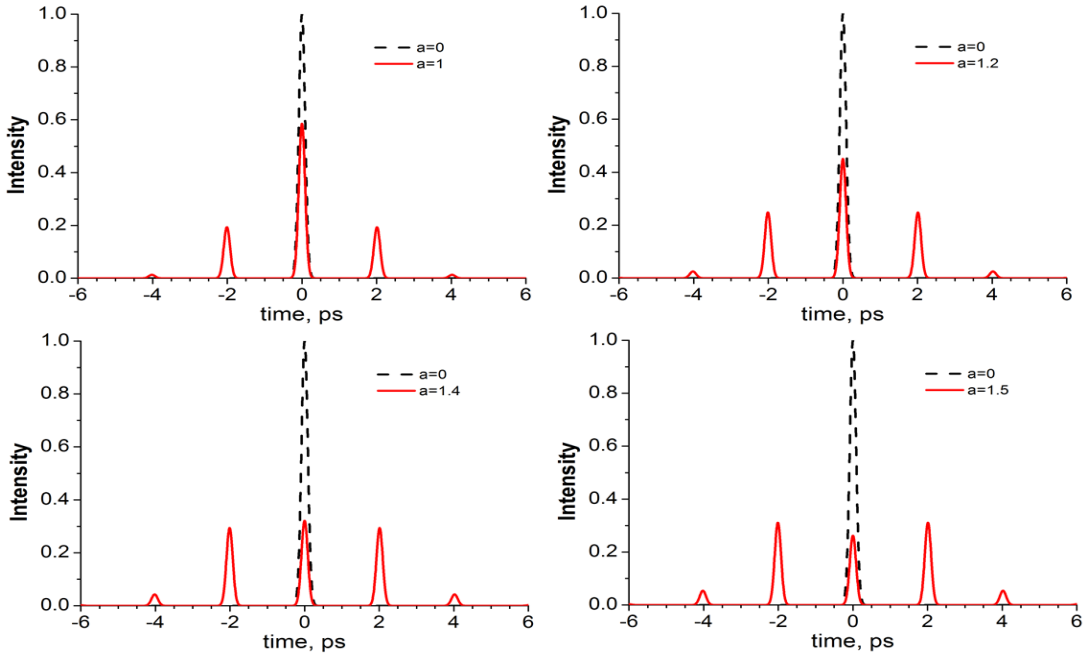

Fig. 8 *Pulses sequence generated by the SLM for different values of the parameter a. The delay τ between the pulses is fixed to 2 ps.*

Such rotational alignment in the filament was used before for polarization shaping of the laser pulses generating high-order harmonics. At the same time, a higher plasma concentration is expected when the intensity of the pulses in the train reaches the ionization threshold because the ionization probability for nitrogen molecules aligned along the laser polarization is about 4 times higher than for perpendicular orientation. Therefore, higher plasma concentration can be created and, correspondingly, higher intensity fluorescence can be observed.

This assumption is confirmed in the experiment on the observation of the backward UV fluorescence yield from the $N_2(C^3\Pi_u)$ excited electronic state of neutral molecular nitrogen as a function of pulse separation presented in Fig.9.

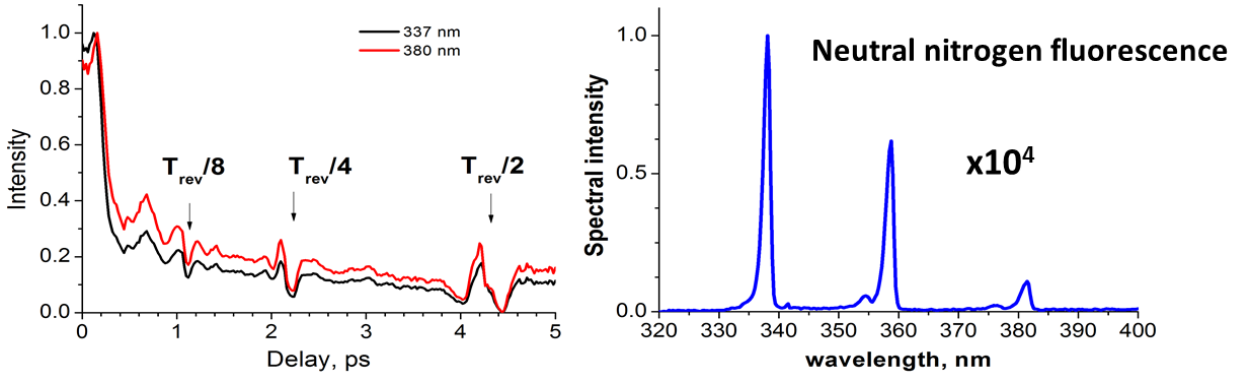

Fig. 9 *Fluorescence intensity at 337 nm and 380 nm, measured in backward direction, as a function of the pulses separation (left). Fractional revivals of the nitrogen rotational wavepacket are assigned. Right – spectrum of the UV fluorescence magnified 10^4 times in comparison to the spectrum of the amplified emission presented in Fig. B5. Nitrogen pressure in the cell 3 bars.*

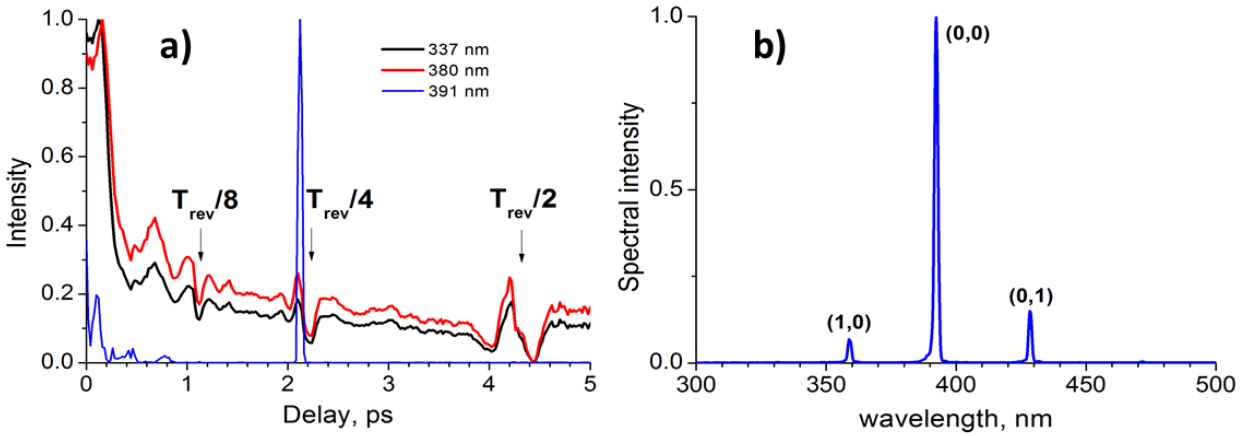

Fig. 10 *a) Intensity of the amplified emission at 391 nm wavelength, detected in the forward direction, as a function of the delay for optimal parameter a=1.6 and pressure 4 bar (blue line); b) spectrum of forward propagating amplified emission with assigned transitions between different vibrational states in N_2^+*

The fluorescence yield peaks at the delays corresponding to a fractional rotational alignment and sharply drops at the delays for fractional anti-alignment. Increase in fluorescence yield in the vicinities of fractional revivals was observed in the whole range of pressures 1-4 bars used in the experiment. Furthermore, the application of a genetic algorithm for a two-dimensional (a- and τ-) optimization of fluorescence results in a strong forward emission at 358 nm, 391 nm and 428 nm (Fig. 10), corresponding to the well-known transitions in the nitrogen molecular ion.

efficient lasing in the real atmosphere conditions.

Progress in WP2 (Standoff CRS detection)

A comprehensive account of the performed activities in WP2 is submitted in deliverable D2.2.

Here we concentrate on the most realistic method of choice and architecture of the final CROSS TRAP apparatus.

The conceptual scheme of a stand-off backward SRS experiment is shown in Fig. 11: it requires the combination of the remotely pumped atmospheric laser (Stokes beam) with an additional frequency-tunable laser beam sent in the forward direction (pump beam). When the frequency difference between the pump and Stokes beams matches a Raman active vibrational transition of the molecule to be detected, then the backward propagating Stokes experiences SRG, enabling sensitive molecular fingerprinting. For spectral resolution, both pump and Stokes need to be narrowband. The N_2 laser is already narrowband; we plan to generate a tunable narrowband pump by spectral compression of femtosecond pulses produced by a visible OPA (690-750 nm) pumped by the second harmonic of the Yb laser initiating the atmospheric lasing.

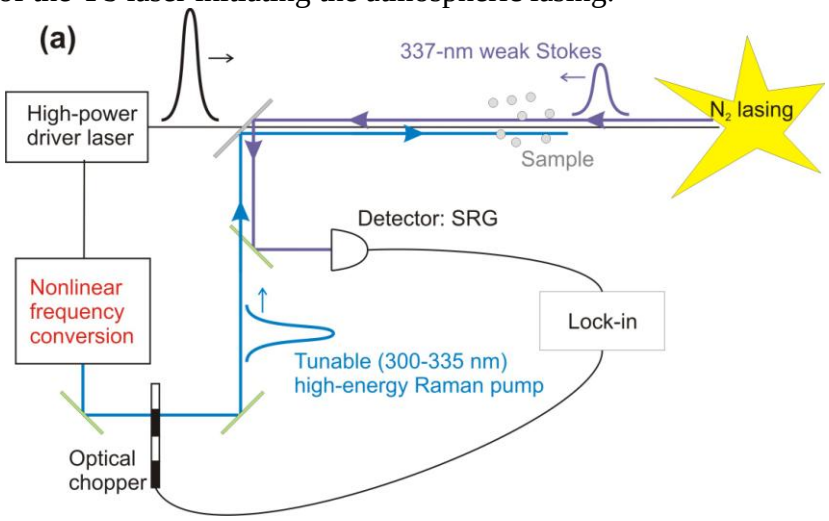

Fig. 11: conceptual scheme of remote atmospheric sensing using backward SRS from an atmospheric laser

Based on the current status in the development of the mid-IR driving source and the prospects for remote nitrogen laser generation in ambient atmosphere, we envisage the following fully functioning CROSS TRAP prototype (Fig.12).

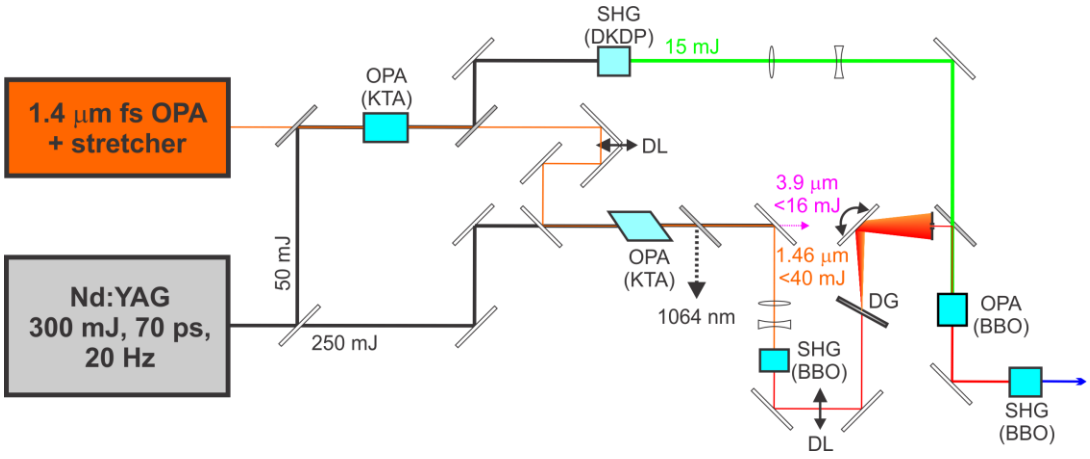

Fig. 12:Expansion of the mid-IR source to include an arm for SRG/SRL pump-probe.

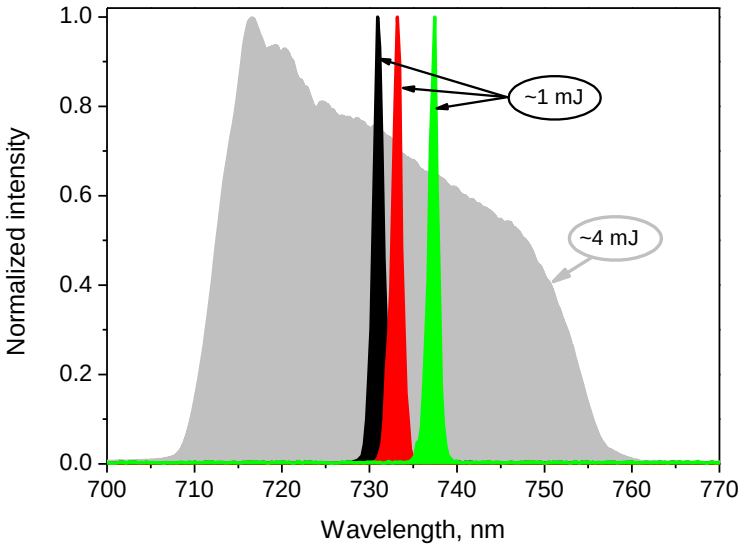

Fig. 13: Demonstration of tunable narrowband pulse generation from the signal pulse arm of the mid-IR source.

Fig.13 shows the achieved prototype result for the generation of pump (or Stokes) pulses to be combined with the 337-nm N_2 radiation excited with the 4-μm arm of the system.

The results of the investigations in WP1 and 2 over the first two years of the project make us confident that a conceptual version of a CROSS TRAP apparatus can be realized within the project life time. The prototype version might not include the integration of the burst mode amplifier (WP4). The addition of the burst mode capability would be essential for entering practical applications with extended-volume targets. However, it might require additional effort after the fundamental challenges of the concept (the use of free-space lasing and coherent Raman sensing schemes) are settled.

Progress in WP3 (Development of the driver laser for remote lasing.)

At the first year evaluation, the project reviewers recommended rethinking the strategy of the project toward the use of low (10-20 Hz) repetition rate laser filamentation sources as opposed to the plan to involve a 1-kHz 100-mJ source which was put forward in the original project proposal. Own observations by the consortium have confirmed presence of accumulation effects that have negatively affected the filament performance at high (0.5—1 kHz) repetition rates. Although the problem with accumulation effects (residual long-lived ions in the beam path, condensation particles, electrostatically charged dust, etc.) would not affect the performance of a scanning laser system where the beam direction is continuously swept in time, there are also significant additional arguments in favor of the reviewers' suggestion to employ lower repetition rates during the development of CROSS TRAP methodology. In particular, one of the most important conclusions of the study of a filament-induced lasing in nitrogen (WP1) was the need for high ponderomotive energy, low optical frequency laser pump pulses. Pulses at the wavelength of 4 μm were found to be

excellently suitable for the task, because, on the one hand, this wavelength is nicely suitable for broadband atmospheric transmission with minimum attenuation and can be obtained using a relatively straightforward OPA technology and, on the other hand, it allows us to generate a filament plasma carrying much hotter electrons. As a result, a richer and more efficient set of plasma-chemical reactions responsible for nitrogen lasing can be accessed with such pulses. Therefore, as explained in Sec. 3.1 of this report, we have redefined the laser parameters of WP3 to develop a 4-μm high-energy pulse parametric source instead of the 1-μm laser source. This move also connects us immediately to the final objective of the laser source development in the project that requires an eye-safe (wavelength >1.5 μm) ultimate laser source. Our preliminary experiments at the wavelength of 4 μm have shown that the energy of mid-IR pulsessuitable for atmospheric filamentation has to be of the level of tens of milli-Joules. Because of the low quantum efficiency of a 4-μm OPA pumped with 1-μm pulses, the 100-mJ pump laser originally envisaged in the project would have been severely underrated. Therefore, instead of pursuing the diode-pumped Yb technology we had to make use of a more conventional flash-lamp pump technology of a picoseconds Nd:YAG amplifier, which is well developed and appropriate for repetition rates under 50 Hz. The development of the mid-IR OPA was assisted by the fact that the TU WIEN lab has previously developed a precursor system for unrelated applications (high-order harmonic generation). This early-stage development was then taken over by WP3 with the aim to scale up the system to the energy level relevant to the CROSS TRAP needs. As a result, over the second year of the project we have nearly doubled the output energy at 4 μm to reach ~12 mJ. Further energy doubling, required to perform filamentation in atmospheric air is expected in 2012. The development of the system is fully reported in Deliverable 3.2. Here we summarize the most important results and implications of WP3.

Figure 14a presents the concept of our hybrid OPCPA based on a combination of a femtosecond CPA front end laser and an OPCPA pumped with picosecond pulses. A detailed adaptation of this scheme for the generation of few-cycle 12-mJ idler wave pulses at the center wavelength of 3.9 μm is given in Fig.14b. The system consists of a three-stage white light (WL) seeded femtosecond OPA pumped by the output of the$Yb:CaF_2$ CPA system, a negative dispersion grating/prism (GRISM) stretcher, a two-stage OPCPA pumped by a picosecond Nd:YAG laser system and a negative-dispersion grating compressor. Below we discuss in detail the working of working of the key subsystems in our scheme characterize their performance.

The chain of parametric amplifiers relies on two pump sources: the initial OPA cascades are pumped by a femtosecond DPSS $Yb:CaF_2$ (Fig.15a) amplifier and the booster OPCPA stages are pumped by and flash-lamp-pumped Nd:YAG (Fig.15b) laser systems. Both the Yb and Nd pump lasers are optically synchronized by a common Yb:KGW Kerr-lens-modelocked seed oscillator (Light Conversion). The front end of the system is a home-built room-temperature $Yb:CaF_2$ regenerative CPA amplifier that drives three cascades of a white-light (WL) seeded optical parametric amplifier (femtosecond KTP OPA). The $Yb:CaF_2$ RA system is seeded by a stretched output of the Yb:KGW oscillator. In order to compensate for the regenerative narrowing and support generation of sub-200 fs pulses, a tunable spectral shaper based on a birefringent KYW

crystal, λ/2 waveplate and a polarizer is installed before the RA. The regenerative amplifier is pumped by two 976-nm laser diodes (DILAS, M1B-976.3-50C-SS2.1) and delivers 1-mJ at a repetition rate of 0.5 kHz. The pump diodes and the Yb:CaF_2 crystal mount are water-cooled. After amplification, the pulses are re-compressed to 190 fs in a compressor based on single transmission grating (Wasatch Photonics) with a groove density of 1700 mm^{-1}.

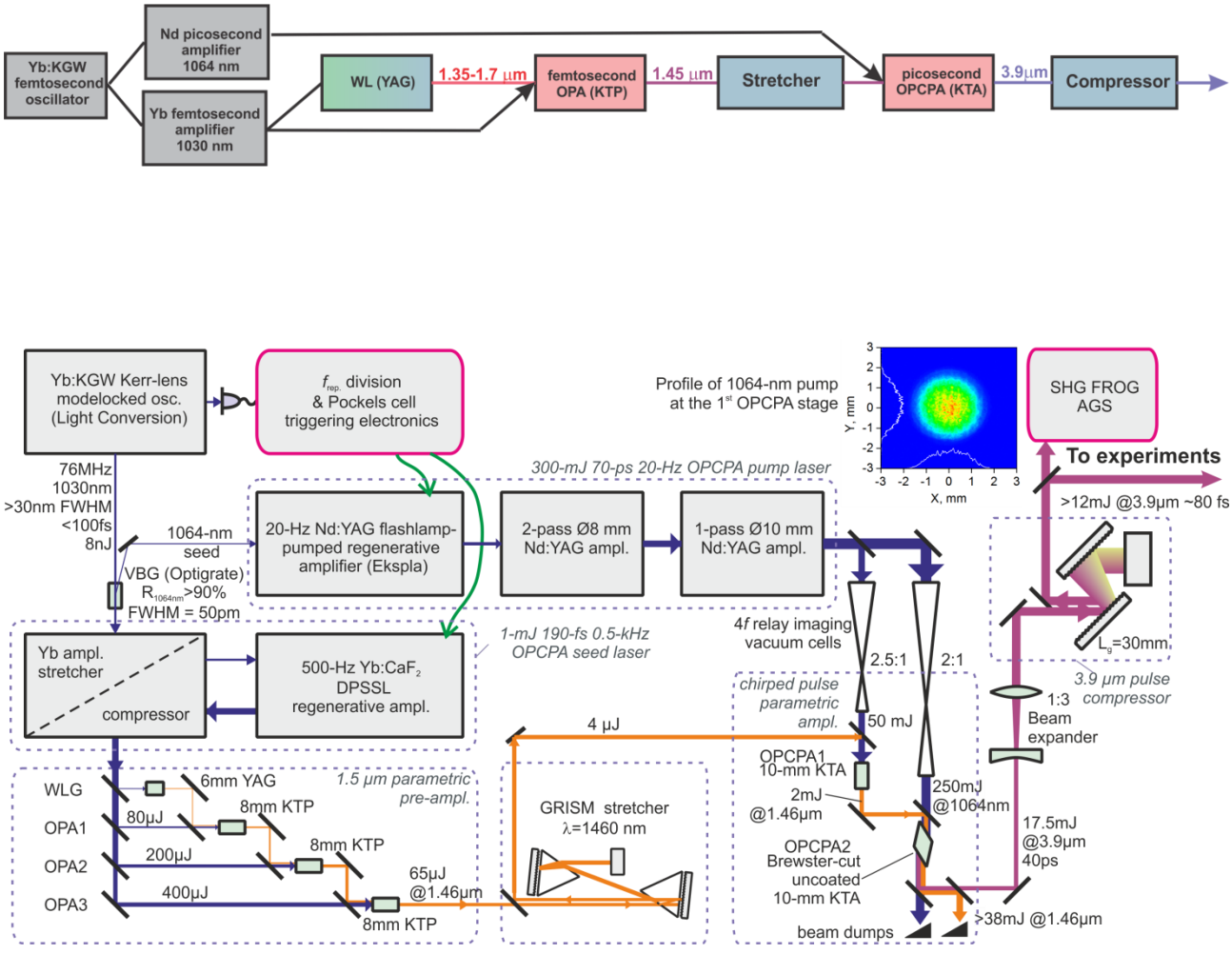

Fig.14. Concept (a) and detailed schematics (b) of the hybrid CPA/OPCPA few-cycle mid-IR system.

A volume Bragg grating with a 50-pm-wide stop band at 1064 nm (OptiGrate Corp.), intercepts the beam at the input of the Yb amplifier stretcher and directs the 1064-nm seed component into the Nd:YAG regenerative amplifier (RA). To limit further nonlinear pulse spectrum broadening in the Nd:YAG system, a 1-mm thick fused silica etalon with 20% reflecting coatings is installed in the regenerative amplifier cavity. In the regenerative amplifier, 1064-nm seed pulses are amplified to a 2 mJ level and, after special filtering, are directed into the first power amplification stage based on a 10-cm long Nd:YAG rod with the diameter of 8 mm. In the double-pass amplifier stage pulse energy is boosted to 100 mJ. The Faraday rotator behind the first power amplifier head is used to compensate thermal stress- induced depolarization. In addition, the thermal lens in the

amplifier rod is compensated by tuning the position of the second lens of the spatial filter (SF in Fig.15b).

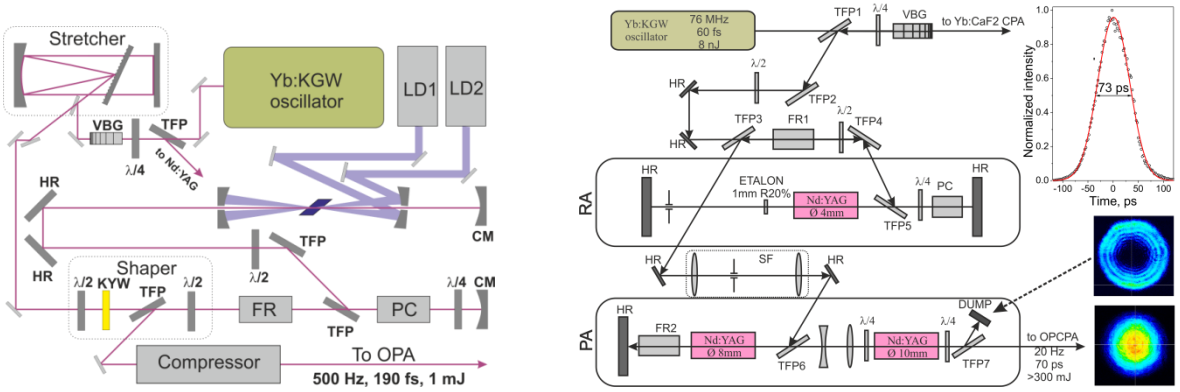

Fig.15. Schematics of femtosecond Yb:CaF_2 (a) and picosecond Nd:YAG (b) laser systems: TFP - thin film polarizer, HR - high reflectivity mirror, CM – curved mirror, VBG - volume Bragg grating, LD – laser diode, FR – Faraday rotator, PC – Poclels cell, λ/2 - half-wavelength retardation plate, λ/4 - quarter-wavelength retardation plate, RA - regenerative amplifier, PA - power amplifier SF - spatial filter. In the top right corner of (b) a cross-correlation function measured with 190-fs, 1030-nm gate pulses from Yb:CaF_2 laser system is shown. In the bottom right corner of (b) spatial profiles of depolarized light (top) and of pump beam (bottom) are presented (for details see text).

Before launching the 100-mJ pulses into the final amplification stage, the beam is expanded in a telescope tuned to compensate the thermal lens induced in the final, 10-cm-long ∅10 mm Nd:YAG rod, which boosts the pulse energy above 300 mJ. Unlike in the preceding, double-pass ∅8 mm amplifier, the beam passes the ∅10 mm laser rod only once which precludes the use of the depolarization compensation scheme with a Faraday in the final 1064-nm amplification stage. To minimize the thermally induced depolarization in this stage, we change the input polarization from linear to circular before the Nd:YAG rod and restore it to linear with a pair of quarter wave plates. This method is helpful in two ways: First, due to a factor of 2 lower intensity of a circularly polarized field in comparison with a linearly polarized one, the accumulation of the B-integral is appreciably reduced. Second, the orthogonally polarized component of the amplified transmitted beam acquires a donut shape (upper inset in Fig.15b) and the component in the input polarization plane has a quasi-supergaussian flattop structure (lower inset). The energy fraction in the donut beam rejected by the polarizer TFP7 (Fig.15b) is only 10%. The energy of linearly polarized output pulses reaches above 300 mJ (6 W at 20 Hz) and can be attenuated by changing the flash lamp voltage and/or flash lamp trigger delay. The output duration is 73 ps FWHM as characterized by a cross-correlation trace between the 1064-nm pulses and femtosecond pulses from the Yb:CaF_2 amplifier (top inset of Fig.15b).

The flattop mode of the 1064-nm beam at the output of the ∅10 mm Nd:YAG rod in the pump booster is relay-reimaged, with the use of evacuated Brewster-windowed cells, onto the two

KTA crystals of the OPCPA stages resulting in ∅4 and 5 mm pump beam spots, respectively, on the input crystal faces.

For the generation of 1.46-μm seed pulses for OPCPA, the output of the Yb:CaF_2 regenerative amplifier is split into four parts by a series of variable beam splitters (consisting of half-wave plates and thin-film polarizers). A 2-μJ portion of the 1030-nm light is used for the generation of WL seed while fractions of 80 μJ, 200 μJ and 400 μJ are utilized for pumping three successive OPA stages based on type II KTP crystals. WL is generated in a 6 mm long, uncoated YAG crystal by focusing the 1030-nm light with a 40-mm lens. The red wing of the WL continuum generated in the YAG crystal extends beyond 1.7 μm (Fig.16).

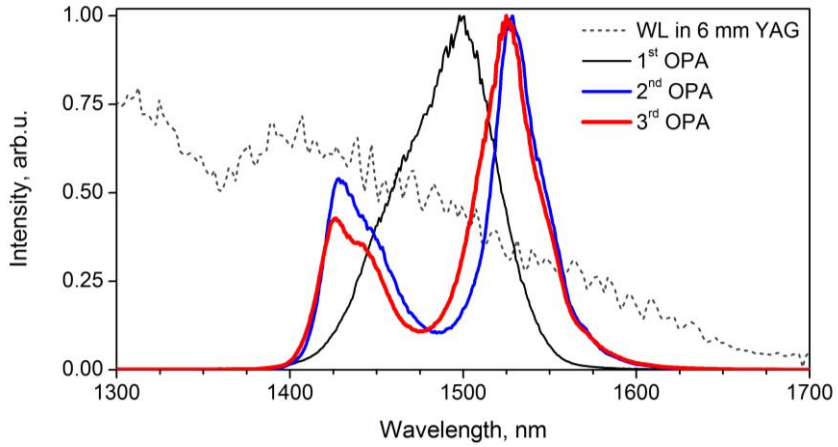

Fig.16. Spectra of the WL generated in YAG crystal and of the output of three OPA.

The generated WL is reimaged onto the KTP crystal of the first OPA stage (6 mm thick KTP crystal, *type II oe-o* (*idler signal-pump*) interaction, $\theta = 43.8^{\circ}$, $\varphi = 0°$). The pump intensity in all three OPA stages is close to 180 GW/cm^2 and is slightly below the level at which parametric superfluorescense is observed. The measured energy of the signal pulses after the third OPA stage is 65 μJ. The pulse-to-pulse stability of the three-stage OPA output is 1.1% rms, and is mainly caused by the fluctuations of the WL-seed and by the pump laser instability. Typical spectra of the amplified signal pulses spanning from 1400 nm to 1600 nm are shown in Fig. 16. The exact shape and the central wavelength of the signal pulse very sensitively determine the resultant bandwidth and energy of the 3.9-μm OPCPA idler. The highest energy and the broadest bandwidth of the mid-IR idler pulses are achieved when the spectrum of the signal pulses seeding the OPCPA are pre-shaped by detuning the phase matching in the OPA stages, as it is shown in Fig. 16.

The Mid-IR OPCPA is seeded at the near-IR signal wavelength. Due to the signal and idler phase conjugation, the stretching of the signal near-IR seed pulses and the compression of the mid-IR idler pulses are both performed by negative-dispersion grating pairs. Brewster-angled LAK16A prisms are installed in the signal pulse stretcher in front of the diffraction gratings, forming a GRISM pair, in order to correct even-order dispersion terms of the idler grating compressor.

The OPCPA consists of two stages based on 10-mm-long KTA crystals, which are transparent at around 4 μm and are suitable for amplification of 1.46-μm signal wave while being pumped at 1064 nm. After the first OPCPA stage only signal pulses are retained for further amplification, whereas the idler pulses are discarded to prevent double seeding of the final amplifier stage. The KTA crystal in the second OPCPA stage has uncoated Brewster-cut faces, which dismisses the problem of optical damage of the AR coatings on the crystal faces. Because of the Brewster angle incidence and exit s-polarized signal pulses experience 25% losses per surface while for *p*-polarized pump and idler the losses are negligible. The second OPCPA stage is pumped by 250 mJ pulses and produces uncompressed 37.5 mJ (with 25% losses accounted for) 1.46-μm signal and 18 mJ 3.9-μm idler pulses corresponding to a >25% overall pump conversion efficiency into the signal and idler.

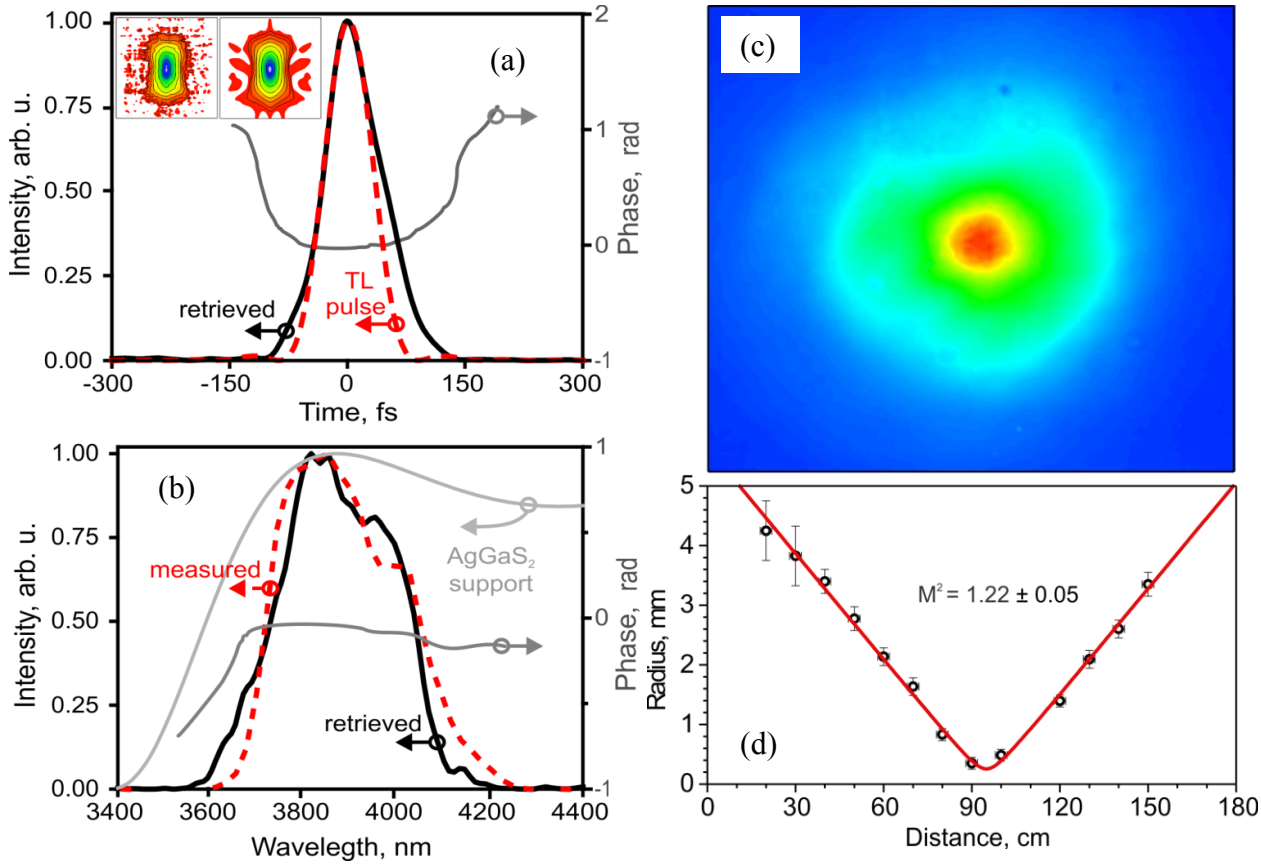

Fig.17 Mid-IR driver performance characterization. a) temporal and b) spectral characteristics obtained from an SHG FROG measurement. c) Measured far-field beam profile. d) M² measurements.

The generated 3.9-μm 18-mJ idler pulses are compressed in a 65%-efficient negative dispersion compressor consisting of a pair of 300 groves/mm gratings, yielding 12 mJ ~80-fs pulses with an rms energy stability of 7.2% as measured for 5000 shots. The instability is mainly caused

by the fluctuation of seed and pump pulse energies, 1.3% and 2.4% respectively, and by the pump beam pointing instability. Despite the highly multimode structure of the 1064 nm pump beam and partial absorption of the generated idler light in the KTA crystal, the 3.9 μm output of the OPCPA has an excellent beam profile (Fig. 17c) with the beam product parameter $M^2 = 1.22$ (Fig.17d).

Temporal characteristics of the 3.9-μm pulses (Fig. 17a) were measured with the second harmonic generation frequency resolved optical gating (SHG-FROG) technique. The sum-frequency signal around 1.9 μm was generated in a 1-mm-thick type I $AgGaS_2$ crystal set at the angle of $\theta = 32.5^\circ$ (Phase-matching curve of the crystal is plotted in the bottom panel of Fig.17b.) As follows from the FROG measurement, the 3.9-μm pulses are compressed to 83 fs whereas the spectrum (Fig.17b) supports 70 fs transform limited (TL) pulses.

Explanation of project resources used in the work package: most of the equipment parts used in the Mid-IR OPA development have been acquired from past funding opportunities of the TU WIEN group, primarily from the start-up funding. This also includes the Joule-class Nd:YAG pump laser upgrade that is due by mid-2012 and should enable nitrogen lasing in air after the energy of the mid-IR pulses is substantially increased. Because the development of the 4-μm OPA has superseded the effort to up-scale the 1-μm diode-pumped laser, there is no impact on the cumulative person-month effort in WP3.

Progress in WP4 (Fiber laser and frequency tuning)

The report on the development of the burst-mode fiber amplifier is provided in Deliverable 4.2. A concise sumary of the main results achieved in WP4 is presented below.

The main objective of the task T4.1 and T4.2 is to develop a high performance ytterbium based fiber laser source that can deliver the high energy pulses required to obtain pump and Stokes signals for the CARS detection scheme. A laser oscillator with a pulse repetition rate of 500 MHz is being developed by MENLO, supplying seed wavelengths for a fiber amplifier system at 1030 nm and 1060 nm, developed by BILU. The fiber amplifier system is specified to produce amplified bursts containing the high repetition rate pulses in the 10 μJ level. The burst repetition rate is 1 kHz.

The main accomplishments under this deliverable are the development of the 500-MHz oscillator by MENLO and the development of a burst-mode Yb-fiber amplifier capable of generating 60-μJ pulses within bursts of extremely uniform energy distribution and 250-ns bursts of 1 mJ of total energy by BILU. By successful collaboration of the project partners, the oscillator has been integrated to the amplifier system and amplified bursts containing pulses of up to 90 μJ individual energy at 500 MHz pulse repetition rate are demonstrated. Such a combined system is demonstrated for the first time, to the best of our knowledge. For the case of the fiber amplifier, the individual pulse energies achieved are record values for integrated fiber systems (i.e., excluding rod type fibers) and it is the first demonstration of a burst mode pulse-pumped fiber laser system, as to date low-repetition-rate burst-mode applications have relied on solid-state laser technology.

The physics of laser oscillators with ytterbium as the favored gain medium are well-known with applications in research, medicine and industry. Nevertheless, usually oscillators are restricted

to pulse repetition rates of a few 100 kHz up to several 10 MHz by limits of cavity design. Due to the fact that a repetition rate of 500 MHz, as required by this project, means an optical path length of only 60 cm, it is a challenging work to design a setup dealing with such a small cavity. With research in optics, mechanics and characterization of physical behavior at high repetition rates, there have been different approaches at Menlo Systems to develop such a laser system.

The final oscillator has been set up as shown in Fig. 18. The pump light is delivered by two fiber-coupled, single-mode pump diodes emitting 650 mW of average power at 974 nm each. The pump light is combined and coupled into the laser ring via a dichroic mirror with a high reflection at 980 nm and high transmission at 1060 nm, offering a sharp edge at 1010 nm in the transmission window.

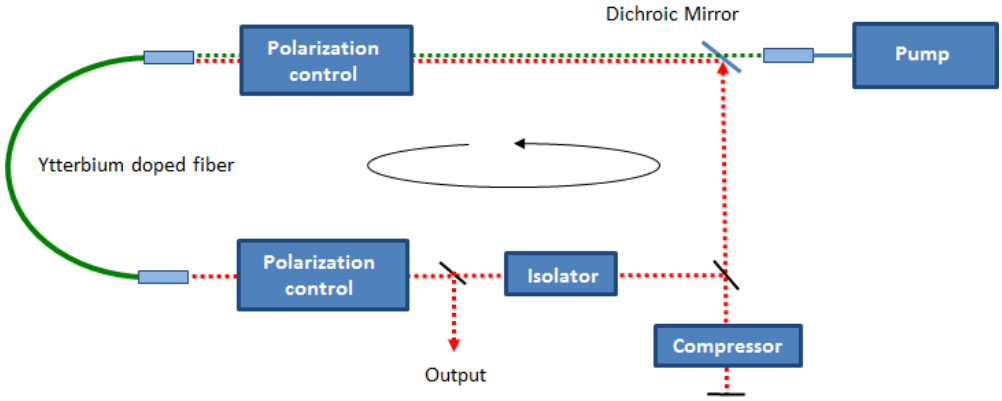

Fig. 18. Dispersion compensated setup of the high repetition rate oscillator. An isolating unit is stipulating the direction of the propagating laser light. A transmission grating compressor unit compensates for the intracavity dispersion. The pump light is coupled into the laser ring via a dichroic mirror.

The laser ring itself includes a fiber which is highly doped with ytterbium, offering an absorption of ~ 3000 dB/m at 975 nm, and a freespace region. The latter includes quarter- and half-waveplates to tune the polarization states of the propagating light. Furthermore, a Faraday rotator in combination with two polarizing beamsplitters represents an isolator, stipulating the direction of the propagating light inside the cavity. The waveplates directly in front and behind the gain-fiber are electronically controlled via an in-house built driver-system. A compressor unit is used to compensate for the intracavity normal dispersion. It consists of two transmission gratings with 1000 lines/mm in Littrow configuration and a retroreflecting end mirror for a double-pass of the incident signal light. The additional GVD is tunable between -6 fs^2 and -32 fs^2. To achieve best modematching results, collimators with the same focal lengths are used at the fiber ends of the gain fiber as well as the passive fiber delivering the pump light. The total length of the fiber ring is 22 cm, including 16 cm of gain fiber, meaning an optical path length of ~ 33 cm inside the fiber ring. The freespace optical path length of the oscillator cavity adds up to 27 cm, thus revealing an overall optical path length of 60 cm, corresponding to a pulse repetition rate of 500 MHz while modelocked (Fig. 19a). The optical pump power launched into the cavity, necessary to achieve stable modelocking, is about 700 mW. The average output power is up to 200 mW, depending on the modelock state. By the applied

dispersion compensated setup, the spectral bandwidth of the emitted pulses is more than 40 nm at a center wavelength of ~ 1045 nm, as can be seen in Fig. 19b.

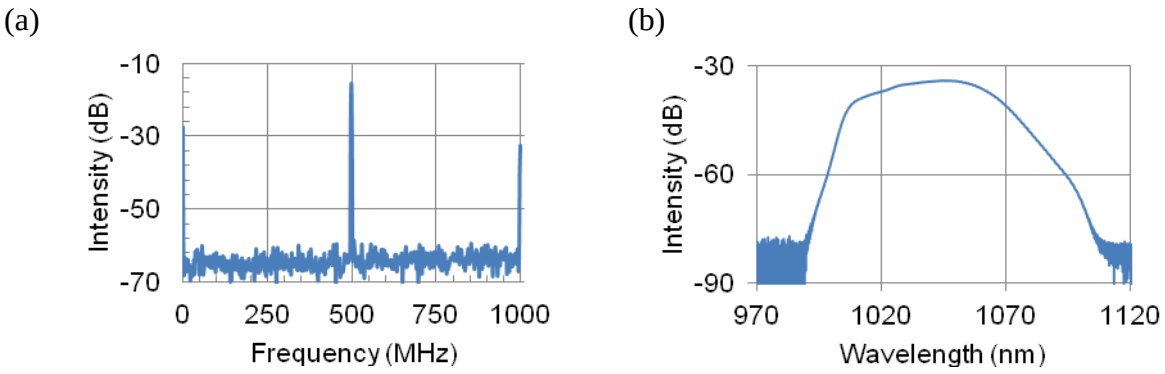

Fig. 19. Radio-frequency spectrum of the outcoupled pulses (a) and optical spectrum of the pulses while modelocked (b) with an FWHM of ~ 40 nm.

After the high repetition rate oscillator has been investigated in detail, it was MENLO's task to put it into a robust structure to ensure long-term stability and portability. An engineering model of the cavity for packaging is shown in Fig. 20. The pump light is delivered via free-space optics (green marking). The polarization controls, the compressor unit and the direction stipulation isolator are in the free-space region of the cavity (red marking). To ensure a complete decoupling of the oscillator from the upcoming amplifier setup, an isolator is installed in the output path of the oscillator (blue marking). If necessary, this cavity chassis is designed to offer space for a piezo-driven mirror for repetition rate stabilization. To enhance the long-term stability of the Laser, the cavity box is temperature stabilized and the gain fiber is chosen to be resistant to photo darkening. Measurements confirm that, once a modelock is found, no further tuning is necessary and the oscillator keeps running over days without any need for readjustments.

As required by the project, it is important for the upcoming CARS-process to have access to seed wavelengths at 1030 nm as well as 1060 nm, to be further amplified in two separate amplifiers. MENLO takes care of providing these two channels directly by the master oscillator. There are different methods that are in principle suitable for spectral filtering to select the required wavelength regions. For example, a custom made WDM with a sharp spectral edge at 1045 nm, placed in the main output port of the oscillator, could split the optical spectrum into two channels. Unfortunately, there was no supplier found for such an optical item. Therefore, a free-space solution has been investigated and designed to fulfill these objectives. A schematic of the developed spectral filter box is shown in Fig. 21a showing its principles.

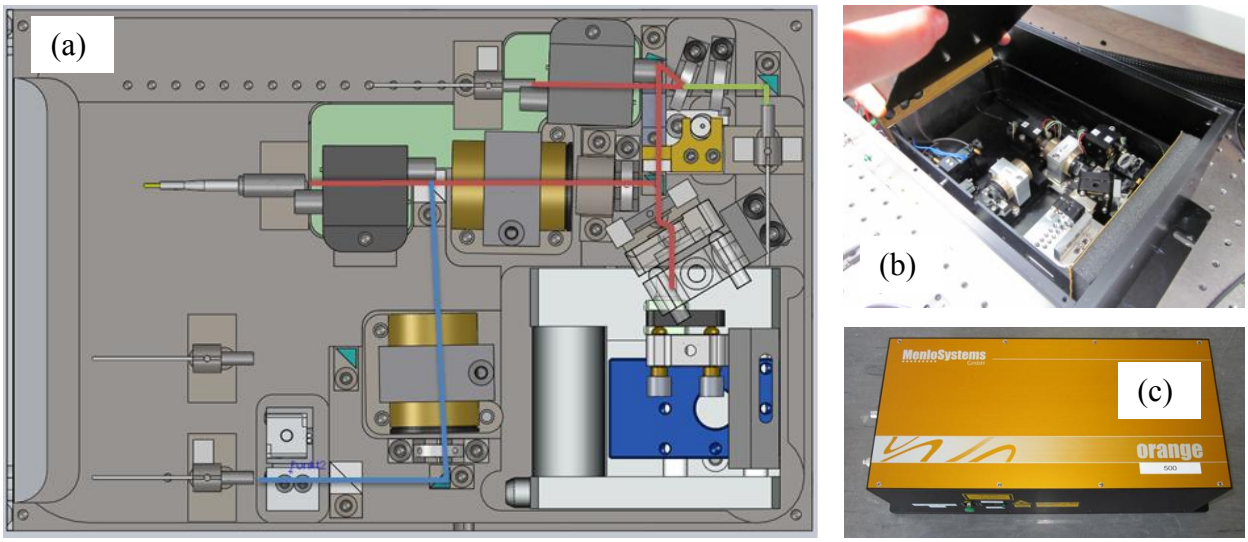

Fig. 20. a) Laser box-design of the 500 MHz oscillator. The pump light is delivered via free-space optics (green marking). The free-space region of the cavity is compact, offering an optical path length of only 27 cm (red marking). The oscillator is protected with an additional isolator in the output path (blue marking) for decoupling from the upcoming amplifier system. b) Photograph of the cavity chassis. c) Photograph of the laser head.

The main output beam is incident on a prism acting as an element with angular dispersion. The wavelengths of the refracted beam are thereby spatially separated and further split into two directions. By tuning the two collimators behind the splitter, one can collect different parts of the spatially chirped light. Fig. 21b shows the optical spectrum of the main output (blue) and each separated channel at 1030 nm (green) and 1060 nm (red). The spectral width at each of the two output channels is > 20 nm with an average output power of ~ 10 mW.

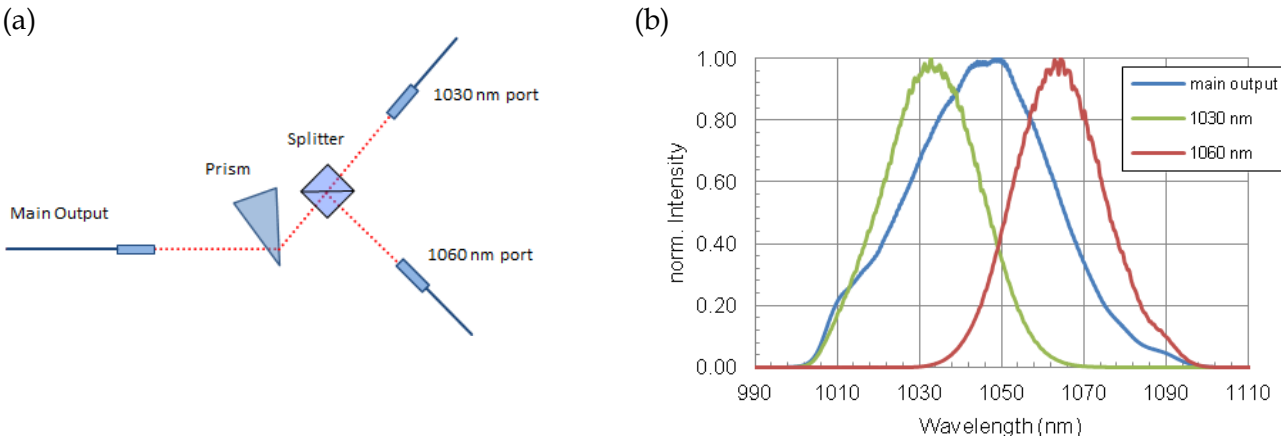

Fig.21. Development of the spectral filter device. Schematics (a) and optical spectra at each output (b); the spectral width is > 20 nm at 1030 nm and 1060 nm each.

In summary, the spectral filter device is capable of separating the main output of the oscillator into two outputs, adjusted for 1030 nm and 1060 nm central wavelength. The fundamental spectral

width of > 20 nm at each channel has been reached so that the spectral requirements by WP4 are fulfilled. Each level of average output power is high enough to seed the burst amplifier stage.

The schematic of the fiber amplifier system before the integration with the MENLO oscillator is shown in Fig. 22. The amplifier system consists of an all-normal dispersion (ANDi) laser oscillator, seeding three stages of core-pumped fiber pre-amplifiers and a double-clad (DC) fiber power amplifier, as well as synchronized pulse picking and pulsed-pumping electronics. A functional diagram of the amplifier system is also given in Fig. 23. The fiber oscillator operates at a repetition rate of 100 MHz and outputs 85 mW, centered at 1035 nm. The oscillator output is polarized with an inline polarization beam splitter (PBS), followed by polarization maintaining (PM) components. The seed pulses, with a bandwidth of 19 nm, are stretched to 360 ps in a 450 m-long PM fiber. The signal is amplified to about 600 mW by two stages of preamplifiers, which are pumped continuously at 976 nm, each with 450 mW. This is followed by a fiber-integrated acousto-optic modulator (AOM), which impresses the desired pulse burst mode. The bursts are amplified in the third preamplifier and thereafter the power amplifier, which are both pumped by pulsed sources in synchrony with the signal burst. For the power amplifier, backward pumping delivered through bulk optics is utilized and the gain fiber is kept short to help minimize the effective nonlinearity and suppress ASE formation. Maximum peak pump power is 23 W and about 70% of it is coupled into the gain fiber with a collimating lens of 2.5 cm focal length and a 10x objective. M^2 of the output beam was measured to be 1.1 at 500 mW output power level.

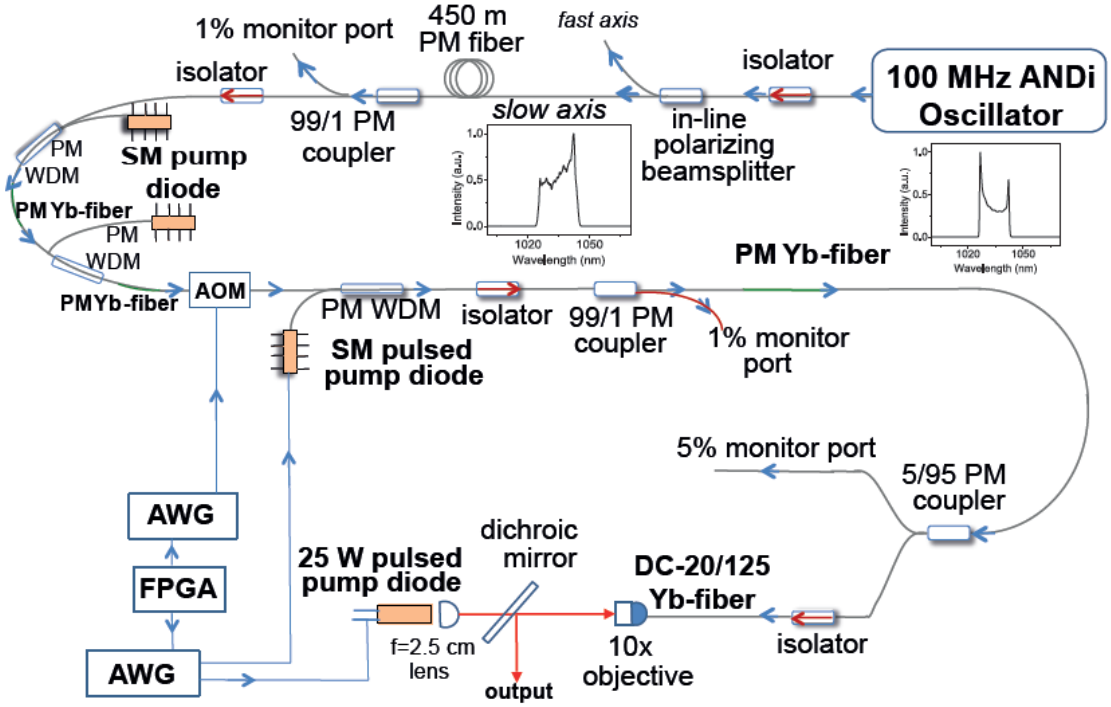

Fig. 22. Schematic diagram of the pulse burst amplifier system; WDM: wavelength division multiplexer; PBS: polarizing beam splitter; PM: polarization maintaining, SM: single-mode, DC: double-clad, AWG: arbitrary waveform generator, FPGA: field programmable gated array. The 100-MHz oscillator was used in the initial testing before the integration of the MENLO seed laser.

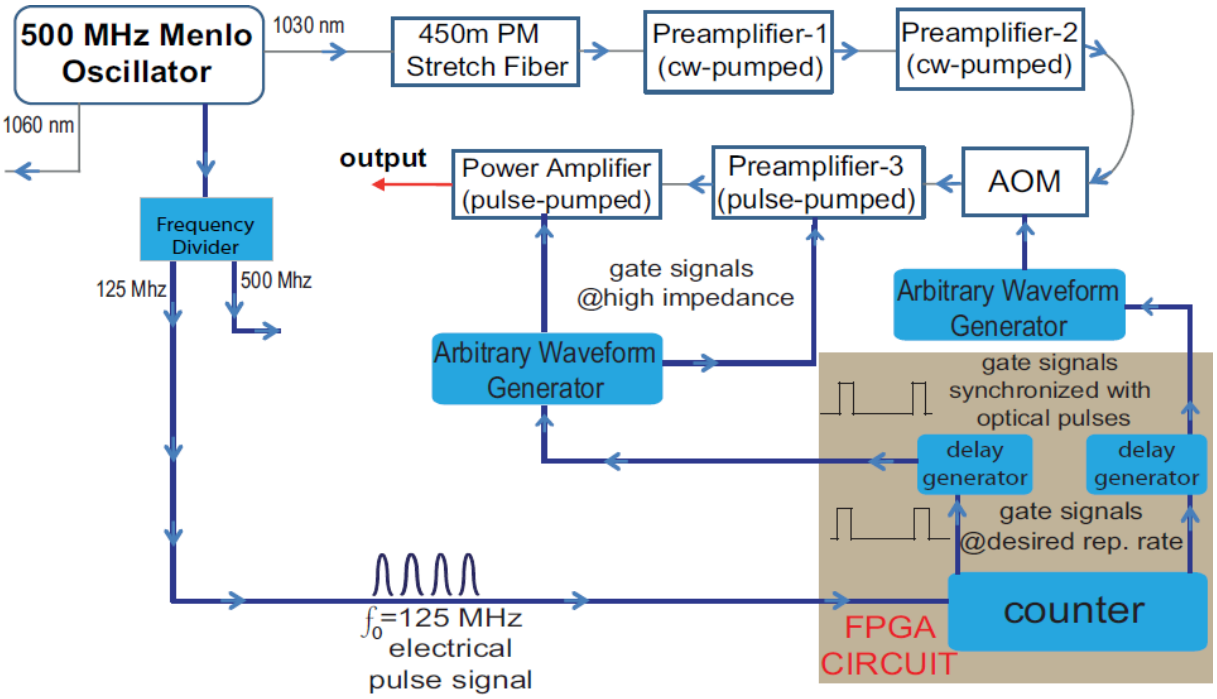

Fig. 23. Functional diagram of the amplifier system after integrating the 0.5-GHz MENLO oscillator in the system..

Two arbitrary waveform generators (AWG) and a field programmable gated array (FPGA) circuit are used to drive the AOM and the pulsed pump diodes (Fig. 23). The FPGA circuit is triggered by the oscillator signal and in turn it triggers the AWG's which drive the AOM and the pump diodes. In this way, phase locking of the pump drive signals and the AOM gate signal to the seed signal, minimizes the jitter of the pulses inside the burst and facilitates the homogenization of the energy distribution within the burst.

After extensive amplifier performance optimization with a temporary 100-MHz repetition rate seeder, the 500-MHz oscillator built by MENLO was integrated with the BILU amplifier system as as shown schematically in Fig. 23. The output spectrum of the laser is separated into two arms, one centered about 1030 nm and the other 1060 nm to provide seeding for the amplified pump and Stokes pulses required by the CRS scheme. The oscillator has an automatic modelocking mechanism and several mode-lock states as discussed above. For the amplification process, we managed to obtain a Gaussian-like spectrum with a FWHM of 40 nm for the main output, where both of the 1030 and 1060 arms have smooth Gaussian-like spectrums of 27 nm and 24 nm FWHM, respectively (Fig. 21,b). A frequency divider which outputs an electrical signal that can be adjusted down to 125 MHz in synchrony with the oscillator signal is provided by MENLO for triggering the FPGA. Since the amplifier system consisted mostly of components built for operation at 1030 nm, the 1030 output arm was used as the seed to test the amplifier performance with the high repetition rate oscillator.

The high repetition rate of the seed signal had two main effects on the amplifier performance. First, in order to obtain high individual pulse energy inside bursts, burst duration has to be kept short and this lowers average signal power and reduces the output power, consequently, per pulse gain is lower, as expected, compared to the 100 MHz seed. Second, the AOM response with a rise and fall time of ~8 ns, each, is slow for the 2 ns period of the signal pulses. This in turn

leads to 4-5 pulses slipping in, at the front and back end of the bursts, and impairs the homogenization process by deteriorating uniformity of pulse energy inside bursts. Especially for short bursts which are used to obtain high individual pulse energy, this effect is significantly intensified.

At the highest amplification level of our system, we obtained around 620 and 600 mW of output power for bursts of 50 and 40 ns duration, containing about 30 and 20 amplified pulses, respectively (Fig. 24a,b). The 1 kHz burst repetition rate indicates total burst energies of 620 and 600 µJ, respectively. The average individual pulse energy is 21 µJ and 30 µJ, while the maximum pulse energy is 27 µJ and 49 µJ, respectively, as a consequence of the non-uniform energy distribution inside the bursts due to the slow response of the AOM. Clearly, the effect is stronger for the shorter burst. As a matter of fact, the calculated standard deviation from the mean pulse energy of 40% and 56%, respectively, reduces to a mere 4.5% for both cases after excluding the AOM effect on both ends of the bursts. The pump to signal conversion efficiency of the power amplifier is about 30% for both.

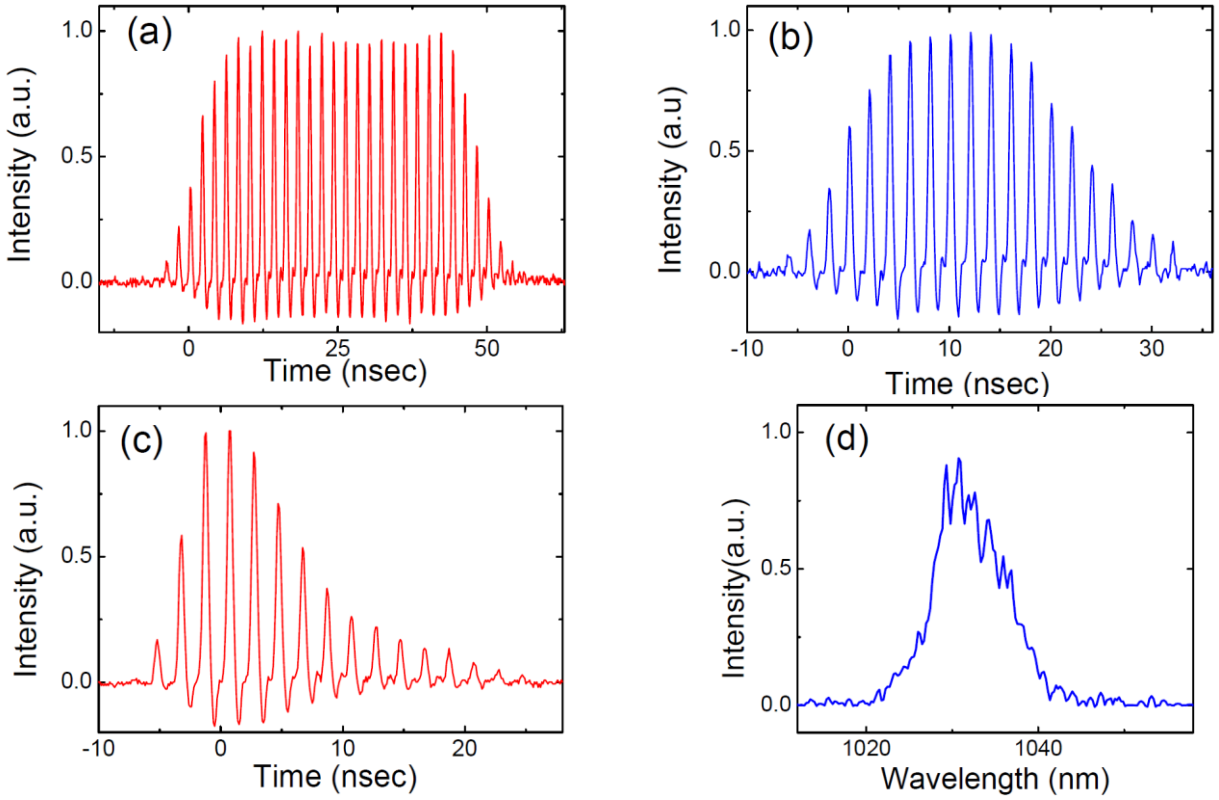

Fig. 24. The amplified pulse bursts: (a) 50 ns duration, 21 µJ average and 27 µJ maximum individual pulse energy, (b) 40 ns duration, 30 µJ average and 49 µJ maximum individual pulse energy, (c-d) 24-ns duration, 37 µJ average and 88 µJ maximum individual pulse energy and the corresponding spectrum, respectively.

Next, to test the limits of individual pulse energy amplification, we used a shorter burst of 24 ns formed with a square gate signal applied to the AOM. A square input burst was used, since any homogenization effort becomes meaningless at this time scale as the total length of the AOM rise and fall times approaches the burst duration. Hence, we obtained a 550 mW output for a burst of approximately 15 pulses with an average of 37 µJ pulse energy, 88 µJ max individual pulse energy

with a very highly nonuniform pulse energy distribution (80% deviation with respect to the mean). The pulse train for this burst of total energy of 550 μJ and the output spectrum is shown in Fig. 24c,d, respectively.

The autocorrelation of high energy pulses from the amplified bursts were measured after compression with the external grating pair of 1500 line/mm groove spacing. The results for the cases of 21, 30 and 37 μJ average pulse energy reported above are shown in Fig. 25a-c, respectively. The inferred pulse durations assuming a Gaussian pulse shape are in the 1, 2 and 5 ps level, respectively. We should stress at this point that, according to our observations in experiments with the amplifier system seeded by the 100 MHz oscillator, the autocorrelation measurement yields pulse durations somewhat longer for pulses in bursts compared to the pulses with a uniform repetition rate with energy equal to the average energy of the pulses in the bursts. One factor causing this effect is definitely that the bursts contain pulses of non-uniform energy which brings about an averaging effect. Considering the high non-uniformity of pulse distribution in these cases, we can expect the measurement result to be at least twice as long compared to the pulse of the same energy with a uniform repetition rate. Unfortunately, with the 500 MHz oscillator as the seed, we are not able to measure amplified pulses at these energy levels with a uniform repetition rate because of the low relative response of the AOM that makes single pulse picking impossible. Further, the large pedestal for the case of 24 ns burst (Fig. 25c) is apparently due to the pulses of maximum energy of ~90 μJ inside these bursts.

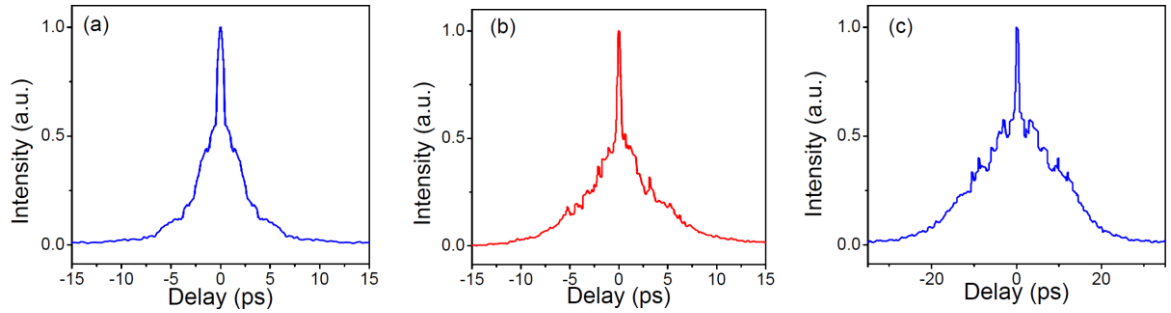

Fig. 25. The autocorrelation results of amplified pulses with average energy of (a) 21 μJ (150 ns burst duration), (b) 30 μJ (250 ns burst) and (c) 37 μJ (250 ns burst).

Integration of the burst amplifier in the final CROSS TRAP system: Two significant deviations from the original proposal have to be taken into account for the integration of the fiber burst mode amplifier in the overall prototype. First, as discussed in the previous section, the final system at the end of the project lifetime will operate at a reduced, 20 Hz repetition rate which is determined by the Nd:YAG pump laser architecture of the eye-safe OPA. Second, the work on the remotely induced gas lasing has established that the backward emitted laser beam from the filament will be in the UV range, almost certainly at 337 nm. This means that in comparison with the original proposal one more frequency conversion (doubling) step will be required for the probe pulse generation. This is the challenge that we will work on during the remaining period of the project. Unfortunately, there is no room to increase the pulse energy of the burst-mode fiber amplifier in view of the limited peak intensity that can safely propagate inside the fiber components. The burst-mode amplifier will

be brought to Vienna after the upgrade of the mid-IR OPA in mid-2012. A particular advantage of the burst-mode amplifier operating at 0.5 GHz repetition rate is that no elaborate synchronization between the OPA (and its pump laser system) and the fiber amplifier is required for the measurement of distributed volumes. The burst mode amplifier will be shipped to Vienna for testing and temporarily installed in the TU WIEN lab by a representative of MENLO or BILKENT.

Narrow bandwidth picosecond pulse formation from broadband output of femtosecond laser.

As described in sec. E3.1, we have decided to continue T4.4 aimed at the development of a spectrally compressed pule for probing of narrowband Raman transitions. This move was motivated by the following considerations: First, our spectroscopy system prototyping in WP2 has revealed the limitation of the spectral pulse compression in a single SHG crystal using the method developed by POLIMI and CL. The particular problem is that for pulses with micro-Joule energies we were not able to increase the pulse duration above 1.5 ps, which translated into appreciable efficiency losses in an SRS experiment because of a poor spectral matching of the pump and probe fields. Second, Light Conversion (LC) has previoously already demonstrated a spectral compressor using a diffraction grating + sum frequency generation. LC was able to adapt this technique to the needs of CROSS TRAP during the 2nd year of the project without requesting additional project resources. A brief report on this development, which is not reflected in other deliverables, is included below.

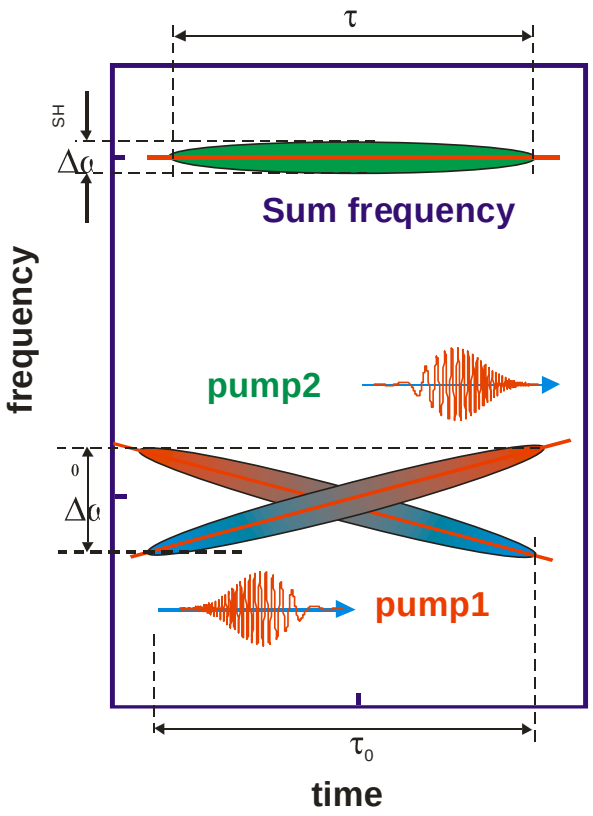

Fig.26 Schematic of narrow band pulse generation when mixing pulses with opposite chirps.

The relation between pulses phases in phase-matched three photon interaction opens an opportunity to control of the spectral bandwidth of the generated pulse. Enhancement of the generated pulse's chirp by summing of pulses with chirps of equal signs has been shown to result in broadening of the spectral bandwidth of the generated pulse as compared to the bandwidths of the initial pulses. Conversely, summing of the pulses with opposite chirps or phase-conjugated signal and idler pulses has been shown to result in bandwidth narrowing.

The principle of narrow bandwidth second harmonic pulse generation using chirped broadband pump pulses is depicted in Fig.25. Let's consider two bandwidth limited pulses with the spectral bandwidth $\Delta\omega_0$ each passing a dispersive medium with different group velocity dispersion. At the output the pulses will be phase modulated and their instantaneous frequencies in the first order approximation will vary in time as: $\omega_1(t) = \omega_c + b_1 t$ and $\omega_2(t) = \omega_c + b_2 t$, where ω_c is the central frequency fundamental pulse, b1 and

b2 are the parameters of linear chirp. The pulses leaving the dispersive medium will be stretched in time depending on the values of b1 and b2 that are proportional to the group velocity dispersion of the dispersive medium.

In case of second harmonic generation when mixing linearly chirped pulses with b1 = -b2 the second harmonic pulse at the zero time delay between fundamental pulses will be chirp-free and its spectrum width correspond to pulsewidth τ of stretched pulses The second harmonic bandwidth compression factor is approximately equal to the factor of fundamental pulse stretching.

Fig.27 Photo of SHBC unit

Employing this principle we have developed second harmonic bandwidth compressor (SHBC) unit (see Fig.27) allowing for generation of narrow bandwidth picosecond pulses using radiation from the femtosecond MOPA system PHAROS as a pump. The sketch of "PHAROS + SHBC" system is presented in Fig. 28. In the experiment, the negatively chirped pulses with spectrum bandwidth of ~ 11 nm from Pharos system was picked up before pulse compressor and were directed to SHBC. Inside SHBC the pump beam was split into two beams of roughly equal power and each of them were directed to identical grating based pulse compressors of negative group velocity dispersion.

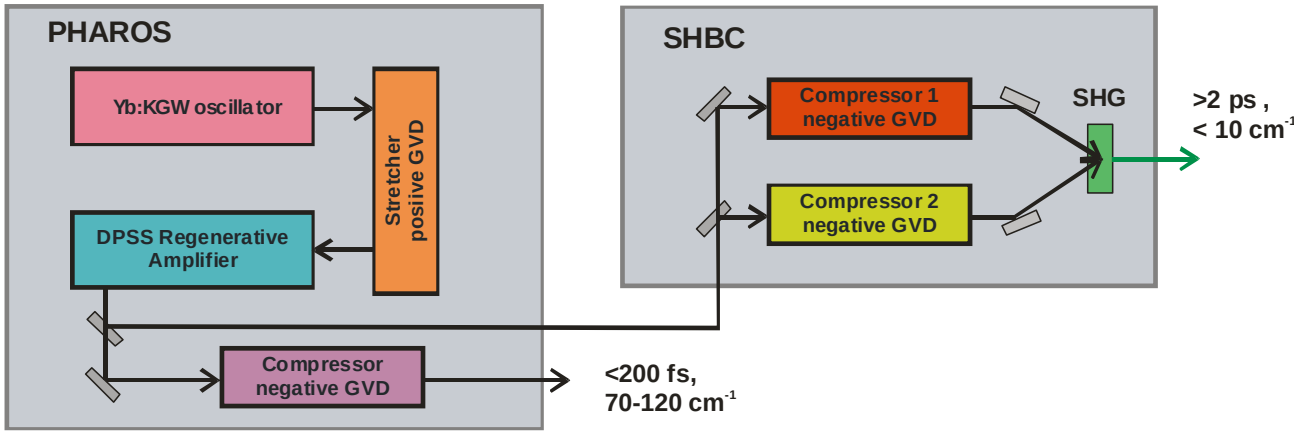

Fig.28 Schematics of experiment

The compressors were adjusted to make the pulses of equal duration but with opposite chirps. One of them was operated in conditions of incomplete pulse compression producing positively chirped pulses of 3 ps. Another one was set for input pulse "over compression" delivering pulses with negative chirp. The pulses from both channels were directed to BBO crystal for second harmonic generation in slightly non-collinear configuration.

The operation of SHBC module was tested using different length crystals for SH generation when pumped with pulses of 500 mW of average power at 10 kHz repetition rate. The table summarizes the measured data.

SH crystal length, mm	SH power, mW	Conversion efficiency (SHBC), %	Conversion efficiency (in SH crystal), %	SH spectrum width, cm^{-1}
0.8	114	23	34	8.7
1	155	31	46	8.7
1.5	185	37	55	8.5
3	181	36	54	7.3

The higher SH spectrum bandwidth compression ratio can be achieved increasing the duration of pump pulses entering SH crystal. To date we have tested SHBC operation with its compressors adjusted for generation of ~ 10ps pulses. In this case the bandwidth of SH pulses at the output of SHBC was around 4 cm^{-1}, but at the expence of sligth distorsions in SH spectrum.
The SHBC unit was tested at different powers of pump beam from PHAROS. The SH pulse power and and total SHBC efficiency using 1.5 mm long BBO crystal as SH generator dependence on delivered pump power is presented in Fig.29.

The short term "PHAROS + SHBC" system energy instability is below 2% while the drift of output average power during 16 hours of operation was below 3% .

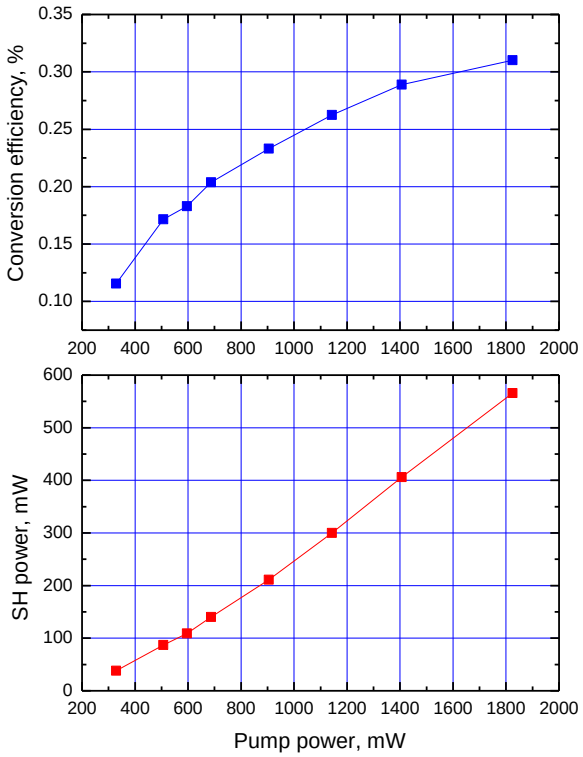

Fig.29. SHBC characteristics for different pump power.

3.2.3 Project management during the period

There were no management problems arising from the Consortium partners. The biggest challenge to date was the registration and enabling of the NEF portal for the periodic reporting. Practically all consortium partners have reported difficulties with using and understanding the system. With the reporting system now finally established, these problems and the corresponding delays are unlikely to be repeated in the future

There is been no change in the composition of the CROSS TRAP consortium.

Two official CROSS TRAP meetings attended by representatives of all Consortium members were held during the first year of the project:

The first review meeting will be held on March 31, 2012 in Milan.

Periodic meeting, Munich 23 Nov. 2011

CROSS TRAP symposium (about 50 participants, 8 invited speakers) was held in Vienna on March 28, 2012. The materials of the Symposium (the book of abstracts) have been submitted online with other project deliverables.

In addition, several meetings where at least 4 groups were represented simultaneously have taken place at the sidelines of various international symposia.

Work package coordination proceeds via bilateral and trilateral conference calls and skype videoconferences. Exchange of scientific equipment and devices normally proceeds via international shipments. Typically laser and mechanical components are shipped between LC and TU WIEN, crystals from CL to POLIMI, fiber components from MSG to TU WIEN.

At the current stage, the Consortium has deviated from the originally planned milestone scheme and abandoned MS6.

The website crosstrap.eu reached its projected functionality in time for the 2nd CROSS TRAP meeting (26 September 2010). The .eu domain has been secured for 1 year and will be extended in September 2011. One of the concerns about the website is the appropriate level of publically accessible information that, on the one hand, should reflect the spectacular progress achieved by the partners in this project and, on the other hand, should not jeopardize the publication/patent application priorities of the Consortium.

We have actively pursued dissemination of the public information on the project and published a paid press release in a Public Service Review of European Science and Technology.

The biggest single task pursued by the management during the second year of the project was the preparation and submission of an INCO extension proposal that was due May 2011 and aimed, at the advice of the project reviewers and the project officer, to extent the initial CROSS TRAP consortium by overseas members—the group of Prof. S.L. Chin (Université Laval, Canada) and Prof. M. Scully (Texas A&M). The submitted proposal has passed the acceptance threshold but was not invited for negotiations with the EC. Written confirmation, that the project has failed to secure funded was issued by the FET office on April 4, 2012.

The tally of the person-months effort during the first two reporting periods is given in the table on the next page:

Person-month effort for personnel employed from the project funding.

Benefi-ciary no.	Benefi-ciary short name	WP1	WP2	WP3	WP4	WP5	WP6	Total per Beneficiary	Year 1	Year 2
1	**TU WIEN**	**35**	4	18		**6**	**2**	**65**	**18**	**19**
2	**POLIMI**		32		25	2	1	**60**	**22.4**	**19.2**
3	**MSG**				22	1	1	**24**	**5.2**	**13.6**
4	**CL**				20	1	1	**22**	**2.3**	**11.3**
5	**LC**			**52**		2	1	**55**	**14.5**	**19.68**
6	**RKU**		**48**			1	1	**50**	**19**	**26**
7	**ILC MSU**	38	20			1	1	**60**	**22.5**	**20.21**
8	**BILKENT**				**48**	1	1	**50**	**13**	**36**
Total		73	104	70	115	15	9	**386**	**111.9**	**139.78**

3.3 Deliverables and milestones tables

Deliverables

TABLE 1. DELIVERABLES

Del. no.	Deliverable name	Version	WP no.	Lead beneficiary	Nature	Dissemination level[2]	Delivery date from Annex I (proj month)	Actual / Forecast delivery date Dd/mm/yyyy	Status No submitted/ Submitted	Contractual Yes/No	Comments
1	Project website		6	TU WIEN	R	PU	6	26/09/2010	Submitted	yes	
2	Report on fs filament characterization at pulse energies ≤5 mJ D1.1	1	1	TU WIEN	R	PU	12	15/03/2011	Submitted	yes	
3	Report on forward CARS using spectral compression D2.1	1	2	UHEI	R	PU	12	15/03/2011	Submitted	yes	

[2] **PU** = Public
PP = Restricted to other programme participants (including the Commission Services).
RE = Restricted to a group specified by the consortium (including the Commission Services).
CO = Confidential, only for members of the consortium (including the Commission Services).
Make sure that you are using the correct following label when your project has classified deliverables.
EU restricted = Classified with the mention of the classification level restricted "EU Restricted"
EU confidential = Classified with the mention of the classification level confidential " EU Confidential "
EU secret = Classified with the mention of the classification level secret "EU Secret "

4	Report on the development and characterization of an Yb gain module with CW laser diode pump power ≥700 W D3.1	1	3	TU WIEN	R	PU	12	15/03/2011	Submitted	Yes	
5	Report on the generation of tunable picoseconds pulses by spectral compression D4.1	1	4	POLIMI	R	PU	12	15/03/2011	Submitted	Yes	
6	Materials of scientific workshop D6.2	1	All	TU WIEN	O	PU	24	28/03/2012	submitted	Yes	
7	Report on the laboratory scale (~10 m) backscatterer D1.2	1	1	TU WIEN	R	PU	24	26/03/2012	Submitted	Yes	
8	Report on background suppression in CARS D2.2	1	2	POLIMI	R	PU	24	26/03/2012	Submitted	Yes	
9	100-W sub 300-fs multipass Yb amplifier D3.2	1	2	TU WIEN	R	PU	24	26/03/2012	Submitted	Yes	
	High performance fiber laser source with novel pulse burst characteristics D4.2	1	4	BILKENT	R	PU	24	26/03/2012	Submitted	Yes	

Milestones

TABLE 2. MILESTONES							
Milestone no.	Milestone name	Work package no	Lead beneficiary	Delivery date from Annex I dd/mm/yyyy	Achieved Yes/No	Actual / Forecast achievement date dd/mm/yyyy	Comments
MS1	**Forward detected CARS using spectral compression**	**2**	**POLIMI**	**15/03/2011**	**Yes**		
MS2	**Tunable picoseconds pulses by spectral compression**	**4**	**POLIMI**	**15/03/2011**	**Yes**		
MS3	Confirmation of back-scattering from a single filament	**1**	**TU Wien**	**25/03/2012**	**Yes**		
MS4	Decision on viability of multiple-filament approach	**1**	**TU Wien**	**25/03/2012**	**Yes**		
MS5	Background suppression in CARS	**2**	**POLIMI**	**25/03/2012**	**Yes**		

MS6	A 100-mJ 1-kHz femtosecond Yb driver laser is developed	**3**	**TU Wien**	**26/03/2012**	**Partial**		**Experimental progress and reviewers suggest a different system is necessary.**
MS7	A burst mode femtosecond Yb fiber laser is developed	**4**	**Bilkent**	**25/03/2012**	**Yes**		

3.4 Explanation of the use of the resources

TABLE 3.1 PERSONNEL, SUBCONTRACTING AND OTHER MAJOR COST ITEMS FOR BENEFICIARY 1 (TU WIEN) FOR THE 2ND PERIOD

Work Package	Item description	Amount in € with 2 decimals	Explanations
1,3	Personnel direct costs	78,639.30	Postdoc salaries for 13 person months (12 PM in WP1, Dr. D. Kartashov, and 1 PM in WP3, Dr. Lingxiao Zhu) Technician salary for 5 months in WP3 (Mr. J. Wild)
1	Other costs	1,196.96	Refurbishment of a turbo pump
5	Other costs	343.88	284.78€ Publication in Optics Letters (OSA) 13.08€ International bank wire transfer charge 3.90€ Loss due to foreign currency exchange rate 42.12€ Sending of a visa invitation to the Turkish project partner via UPS
1,3,5	Travel costs	3717.85	1st year CROSS TRAP review meeting, Milan, 31 March 2011, (participants A. Pugzlys, D. Kartashov, T. Balciunas) Ultrafast Optics, Monterey + stop at Princeton Univ. (visit to Prof. M. Shneider) 25.09—0.6.10.2011- traveler Dr. D. Kartashov Lisbon workshop, 09.10.2011, traveler Dr. Daniil Kartashov – Invited talk on CROSS TRAP related scientific work at the 3rd Conference on Ultraintense Laser Science, Lisbon, Portugal October 10-13, 2011
	Indirect costs	50,338	
	TOTAL COSTS[3]	134,236	

[3] Total costs have to be coherent with the costs claimed in Form C.

TABLE 3.2 PERSONNEL, SUBCONTRACTING AND OTHER MAJOR COST ITEMS FOR BENEFICIARY 2 (POLIMI) FOR THE PERIOD

Work Package	Item description	Amount in € with 2 decimals	Explanations
2,4	Personnel direct costs	64848,81	PhD student (V. Kumar) and researchers (M. Marangoni, G. Cerullo) salaries for 19.2 person months (14.2 PM in WP2 and 5 PM in WP4)
	Consumables	20268,42	Optical components (crystals, mirrors, filters, lenses) and electronic components, diode laser head, journal publication charges, management expenses related to the organization of the first year review meeting (catering costs, photocopies, binding expenses,…)
	Investment	5931,25	Depreciation costs for: personal computers, acousto-optic modulator, optical cavity for gases, laser power supply and controller
	Travel costs	4382,39	G. Cerullo: conference Advanced Solid State Photonics (Istanbul, February 13-17, 2011) € 1460.20 M. Marangoni: conference CLEO Europe 2011 (Munich, May 23-25 2011) € 1085.00 D. Brida: conference CLEO Europe 2011 (Munich, May 23-25 2011) € 1157.80 M. Marangoni: CROSS TRAP 18 month meeting (Munich, November 23, 2011) € 679.39
	Total direct costs	95.430,87	
	Indirect costs (overheads)	58623,32	
	TOTAL COSTS[3]	154054,19	

TABLE 3.3 PERSONNEL, SUBCONTRACTING AND OTHER MAJOR COST ITEMS FOR BENEFICIARY 3 (MSG) FOR THE PERIOD

Work Package	Item description	Amount in € with 2 decimals	Explanations			
WP 4	Personnel direct costs	58.030,69	RTD:			
			Name	Months on Project	Hours on Project	Project cost
			R.Holzwarth	02/11-1/12	60	3.981 €
			H. Hoogland	02/11-1/12	1.675	49.367 €
			U.Göhler	01/12	60	1.593 €
			Management			
			B. Hohenthaner	02/11-1/12	50	3.090 €
			Total			**58.031 €**
WP 4	Direct costs	17.771,29	Material costs to build a laser system - electronics - optical components - mechanical components - laser diodes - **Subtotal**			 4.901 € 5.424 € 4.379 € 1.980 € **16.684 €**
			Travel: R. Holzwarth (Milan, 30.-31.03.2011, first year review meeting, flight costs for 2)			960 €
			Travel: H.Hoogland (Milan, 30.-31.03.2011, first year review meeting, without flight costs)			127 €
			Total			**17.771 e**
	Indirect costs	45.481,19				
	TOTAL COSTS[3]	**121.283,17**				

TABLE 3.4 PERSONNEL, SUBCONTRACTING AND OTHER MAJOR COST ITEMS FOR BENEFICIARY 4 (CL) FOR THE PERIOD

Work Package	Item description	Amount in € with 2 decimals	Explanations
4,5	Personnel costs	59941.42	Engineering staff salaries for 11.3 person months (11.1PM in WP4 and 0.2 PM in WP5) Dr Corin Gawith, CTO: 0.3MM WP4, 0.2MM WP5 Dr Huw Major, R&D Engineer: 8.0MM WP4 Dr Hazel Hung, Laser Engineer: 2.5MM WP4 Karl Morris, Technician: 0.3MM WP4
	Other direct costs	8108.42	Materials etc €5350.30 raw crystal wafers €1179.31 oven parts €54.54 cotton buds €48.07 shipping (from suppliers) €157.21 shipping (to partners) Travel €636.94 Y1 review meeting (Milan 30/03/2011 to 31/03/2012, Corin Gawith&Huw Major) €682.05 WP4 technical review meeting at CLEO (Munich 25/05/2011 to 26/05/2011, Corin Gawith&Huw Major)
	Indirect costs (overheads)	40829.90	
	TOTAL COSTS[3]	108879.74	

TABLE 3.5 PERSONNEL, SUBCONTRACTING AND OTHER MAJOR COST ITEMS FOR BENEFICIARY 5 (LC) FOR THE 2ND PERIOD

Work Package	Item description	Amount in € with 2 decimals	Explanations
3,5	Personnel direct costs	32721,10	Salaries of company personnel total 19.68 PM *WP3* L. Giniūnas 0,24 A. Varanavičius 0,21 V. Čiapas 0,53 J. Pocius 0,10 J. Boskaitė 0,76 G. Čyvas 1,05 M. Bardauskas 1,05 K. Jasionis 1,05 O.Tchagapsova 1,38 V. Kinderis 1,57 P. Mišeikis 1,16 V. Macedunski 1,05 I. Mikulskas 1,05 D. Dargis 1,05 M. Barkauskas 1,05 A. Dimavičius 1,05 A. Rimšelienė 1,05 R.Vaižmužytė 0,53 R.Karkockas 0,29 D.Mikalauskas 0,34 V.Mikėnas 0,81 D. Grigaitis 0,33 D.Pagarielovienė 1,05 R.Danielius 0,24 *Total PM in WP3 18,99* *WP5* A. Varanavičius 0,43 J. Boskaitė 0,26 *Total PM in WP5 0,69*
	Consumables	9132,75	Components for development of driver laser (optical and mechanical components, detectors,). Major costs: Yb: doped laser crystals- 1537,88 Eur, BBO crystals - - 1755,10 Eur
	Travel costs	678,78	A.Varanavicius trip to Milan 2011.03.30-04.01 to CROSSTRAP first year review meeting 678,78 Eur

	Total direct costs	42532.63	
	Indirect costs (overheads)	25519,57	
	TOTAL COSTS[3]	68052,20	

TABLE 3.6 PERSONNEL, SUBCONTRACTING AND OTHER MAJOR COST ITEMS FOR BENEFICIARY 6 (UHEI) FOR THE PERIOD			
Work Package	Item description	Amount in € with 2 decimals	Explanations
2,4	Personnel direct costs	78475,72	J.M. Möhring Feb.2011-Dec.2011 (11M) T. Buckup Feb.2011-Jan.2012 (12M) H. Skenderovic Nov.2011-Jan.2012 (3M) 26 person months (WP2)
	Consumables	22181,73	Optical components (crystals, mirrors, filters, lenses) and electronic components, chemicals
	Investment	216,71	Personal computers
	Travel costs	4062,04	M. Motzkus: Milano CROSS TRAP meeting, Italy T.Buckup: Meeting: Time-Resolved Vibrational Spectroscopy XV , Ascona, Switzerland M.Motzkus: Meeting CROSS TRAP, Munich, Germany T.Buckup: DPG Meeting, Dresden, Germany J.Möhring: DPG Meeting, Dresden, Germany J. Möhring: Joint research experiment, Wien, Austria
	Total direct costs	104936,20	
	Indirect costs (overheads)	54933,00	
	TOTAL COST	159869,20	

TABLE 3.7 PERSONNEL, SUBCONTRACTING AND OTHER MAJOR COST ITEMS FOR BENEFICIARY 7 (ILC MSU) FOR THE PERIOD

Work Package	Item description	Amount in € with 2 decimals	Explanations
1,2	Personnel direct costs	59456.90	Total 20.21 productive months WP1: 12.68 productive months : Prof. A.Zheltikov, Group Leader - 2.22 Dr. D.Sidorov-Biryukov, Sen. Researcher -2.7 Dr. E.Serebryannikov, Researcher -1.96 Dr. A.Mitrofanov, Researcher - 1.18 Mr. A.Voronin, Jun.Researcher - 2.42 Mrs. L.Amitonova, Jun.Researcher, p.g.stud. -2.2 WP2: 7.53 productive months Dr. A.Fedotov, Senior Researcher - 2.76, Dr. I.Fedotov, Researcher - 2.57 Mr. A.Lanin, Junior Researcher, p.g.stud. -2.2
	Consumables	557.43	Connectors, fibers accessories, cleaning pads, laser module
	Investment (Service)	549.85	Spectrometer repairing
	Travel costs	4823.15	A.Zheltikov (06.02.2011 – 08.02.2011, Germany, seminar on Standoff Detection, work on WP1) - 499.89 € A.Zheltikov (29.03.2011 – 02.04.2011, Italy-Germany CROSS-TRAP project meeting) - 818.56 € A.Zheltikov (18.06.2011 – 20.06.2011 Germany, seminar on Standoff Spectroscopy work on WP1) – 599.96 € A.Zheltikov (22.11.2011 – 26.11.2011, Germany, CROSS-TRAP project meeting) – 781.43 € A.Zheltikov (28.11.2011 – 12.12.2011, USA, seminar on Nonlinear Standoff Spectroscopy, work on WP1) – 830.90 € A.Zheltikov (16.12.2011 Saint-Petersburg, Russia, consultation on WP1) – 149.78 € A.Zheltikov (07.01.2012 – 14.01.2012, Germany, CROSS-TRAP project meeting) – 1142.63 €
	Bank Charges	322.00	Charge for money transfer (200 €) and charge for currency exchange (122 €)
	Total direct costs	65709.33	
	Indirect costs (overheads)	13141.87	
	TOTAL COSTS[3]	78851.2	

TABLE 3.8 PERSONNEL, SUBCONTRACTING AND OTHER MAJOR COST ITEMS FOR BENEFICIARY 8 (BILU) FOR THE 2ND PERIOD

Work Package	Item description	Amount in € with 2 decimals	Explanations
4	Personnel direct costs	69758.53	Post Doctoral Researchers (Hamit Kalaycıoğlu, Ihor Pavlov and Parviz Elahi) salaries for 12 months (WP4)
	Consumables	5648.93	Optical components from Thorlabs
	Travel costs	2398.41	Hamit Kalaycıoğlu and Omer Ilday: trip to Milano, Italy for CROSS TRAP meeting Hamit Kalaycıoğlu: trip to international conference Advanced Solid State Photonics (ASSP) for an invited talk Ihor Pavlov: trip to international conference CLEO Europe for an invited talk
	Total direct costs	77805.87	
	Indirect costs (overheads)	46683	
	TOTAL COSTS[3]	124488.87	